DESIGN OF AN ADAPTIVE AUTOPILOT FOR AN EXPENDABLE LAUNCH VEHICLE

by

CLINTON E. PLAISTED
B.S. Virginia Polytechnic Institute and State University, 1999

A thesis submitted in partial fulfillment of the requirements
for the degree of Master of Science in Aerospace Engineering
in the Department of Mechanical, Materials, & Aerospace Engineering
in the College of Engineering and Computer Science
at the University of Central Florida
Orlando, Florida

Spring Term
2008

ABSTRACT

This study investigates the use of a Model Reference Adaptive Control (MRAC) direct approach to solve the attitude control problem of an Expendable Launch Vehicle (ELV) during its boost phase of flight. The adaptive autopilot design is based on Lyapunov Stability Theory and provides a useful means for controlling the ELV in the presence of environmental and dynamical uncertainties.

Several different basis functions are employed to approximate the nonlinear parametric uncertainties in the system dynamics. The control system is designed so that the desired response to a reference model would be tracked by the closed-loop system. The reference model is obtained via the feedback linearization technique applied to the nonlinear ELV dynamics. The adaptive control method is then applied to a representative ELV longitudinal motion, specifically the 6th flight of Atlas-Centaur launch vehicle (AC-6) in 1965. The simulation results presented are compared to that of the actual AC-6 post-flight trajectory reconstruction.

Recommendations are made for modification and future applications of the method for several other ELV dynamics issues, such as control saturation, engine inertia, flexible body dynamics, and sloshing of liquid fuels.

"At the touch of love everyone becomes a poet" – Plato. I dedicate this composition to my wife, Gretchen, for all her encouragement, understanding, patience, and most of all, unconditional love. Her cheerfulness during my times of anxiety, tolerance of my absences, and chastisement of my procrastination has led directly to all my successes.

ACKNOWLEDGEMENTS

This work would have not been completed without the help and support of several individuals. First and foremost, I thank my advisor Dr. Leonessa for his passionate advice and support he gave to me along the way. I could not have achieved success without his hours of teaching me the principles of adaptive control. His willingness to work with a part-time student, even when I was remotely located, was greatly appreciated. Thank you, Alex.

I would also like to thank my committee members Dr. Kuo-Chi Lin and Dr. Chengying Xu for their willingness to review my work and provide valuable comments. I am grateful to my employer, a.i. solutions, Inc. for their financial assistance and the department of Mechanical, Materials & Aerospace Engineering for its support of my education at the University of Central Florida.

TABLE OF CONTENTS

LIST OF FIGURES

LIST OF TABLES

LIST OF ACRONYMS/ABBREVIATIONS/NOTATIONS

3-DOF	Three Degrees of Freedom (Motion)
AC-6	Sixth Flight of the Atlas-Centaur Launch Vehicle
ALS	Advanced Launch System
BECO	Booster Engine Cut-Off
C_A	Coefficient of Axial Aerodynamic Force
C_{N_0}	Coefficient of Normal Aerodynamic Force Due to Zero Angle-of-Attack
C_{N_α}	Coefficient of Normal Aerodynamic Force Angle-of-Attack
CG	Center-of-Gravity Location on Vehicle
CP	Center-of-Pressure Location on Vehicle
ELV	Expendable Launch Vehicle
I_{yy}	Pitch Moment of Inertia
$\dot{I}_{yy}$	Time-Derivative of Pitch Moment of Inertia
ITAR	International Traffic in Arms Regulations
l_α	Distance from CG to CP
l_c	Distance from CG to Engine Gimbal Station
LTI	Linear Time-Invariant
m	Vehicle Mass

MRAC	Model Reference Adaptive Control
NASA	National Aeronautics and Space Administration
q	Rotational Rate of the Vehicle Body Axes
$\dot{q}$	Rotational Acceleration of the Vehicle Body Axes
$\overline{q}$	Dynamic Pressure
PI	Proportional-integral (control)
PLF	Payload Fairing
S_{ref}	Reference Area (Cross Section Area)
SRM	Solid Rocket Motor
TVC	Thrust Vector Control
T_c	Control Thrust
T_s	Static Thrust
U_I	Inertial Velocity Component in X_I Direction
$\dot{U}$	Acceleration Component in x_b Direction
USAF	United States Air Force
V_I	Inertial Velocity Component in Y_I Direction
V_r	Relative Speed
$\dot{W}$	Acceleration Component in z_b Direction

W_E	Wind speed in East direction
x_b	Body Axis of Vehicle (Through Nose)
X_I	Inertial Position of Vehicle CG (Up Direction)
X-15	Experimental Test Aircraft (Hypersonic/Spaceflight)
Y_I	Inertial Position of Vehicle CG (East Direction)
z_b	Body Axis of Vehicle (Perpendicular to x_b and Points East on Launch Pad)
α	Angle-of-Attack
γ	Flight-Path Angle
δ_p	Engine Gimbal Angle for TVC
θ	Vehicle Body Angular Attitude in Pitch-Plane
θ_e	Angular Attitude Error in Pitch-Plane
$\dot{\theta}_M$	Measured Vehicle Body Angular Rate
c_I	Integral Control State (Baseline Control System)

CHAPTER 1: INTRODUCTION

This study investigates the use of a Model Reference Adaptive Control (MRAC) direct approach to solve the attitude control problem of an Expendable Launch Vehicle (ELV) during its boost phase. The adaptive autopilot design is based on Lyapunov Stability Theory and provides a useful means for controlling the ELV in the presence of environmental and dynamical uncertainties.

1.1 Motivation

Adaptive control techniques began to emerge in the mid 1950's for applications of flight control [1]. Supersonic flight was still a rather new phenomenon, hypersonic flight was just starting to be researched, and ballistic missiles were being developed to deliver weapons from space. When the Soviet Union launched the first Sputnik satellite, many aerospace research and development programs were initiated and/or infused with funding. One particular program, the experimental hypersonic research program of the X-15, would provide a test bed for adaptive flight control.

The current Space Shuttle orbiter owes many of its technical achievements to the X-15 program. The X-15 had the first aerodynamic/reaction control system, which allowed it to transition from atmospheric flight to space fight and back. The third X-15 aircraft had an adaptive control system developed by Honeywell [2] that was a model following adaptive variable gain, rate command augmentation system and autopilot. The system was installed in series with the basic X-15 hydromechanical control system in the same general arrangement as the basic stability augmentation system which it replaced [3]. The adaptive control system flew many times before a disastrous flight test accident took the life of a pilot in November 1967.

While many factors were found to have contributed to the failure, it was established that the adaptive control system did not normally reduce the gains and they drifted to critical values. Due to the control actuation also being saturated, a limit-cycle developed that put the vehicle in accelerations that exceeded its structural limits.

An important outcome of that accident was the questioning of the use of adaptive control over that of conventional (and simpler) gain/filter scheduling at several fixed intervals in the flight envelope [4]. This philosophy would prevail in industry over much of the next 25 years, until rigorous stability proofs and architectures to prevent parameter drift were revisited. Even with the X-15 failure, 65 previous flight tests demonstrated that the adaptive control system provided nearly invariant response at essentially all aerodynamic flight conditions. They also proved that a priori knowledge of the aircraft aerodynamics was not required and configuration changes were adequately compensated. These are benefits of adaptive control that can be exploited today.

Most current expendable launch vehicles (ELVs) evolved from original designs from the 1950's and 1960's [5], [6]. They employ time dependent gain/filter scheduling across a large flight envelope as the vehicle is accelerating after launch. Control actuation is achieved by gimbaled nozzles that vector the thrust from the engines. Evolved designs usually include changing external mold lines, such as adding solid rocket motors (SRMs) for increased performance or changing payload fairings (PLFs) for enhanced payload capabilities. In addition to aerodynamic changes of the ELV configurations, there are external disturbances of wind gusts that affect the controllability of the vehicle and launch opportunities throughout the year. For example, engine actuator saturation may occur near maximum dynamic pressure portions of the

trajectory with unknown wind gusts. Lastly, all large ELVs deal with uncertain dynamics such as time varying mass properties, aero-elasticity (bending) and fuel slosh that may cause stability or performance issues that gain/filter scheduled autopilots may not easily solve. Adaptive control schemes can be investigated to alleviate these problems with a unified framework using the most recent advances in the theory.

The direct MRAC scheme has potential cost savings by reducing the amount of wind-tunnel testing needed as well as eliminating the need for maintenance of large aerodynamic databases. The ability to design and develop a single control system design for several vehicle variants reduces design complexity as well as cost. MRAC also has shown robustness to uncertainties with sometimes improved and more predictable performance.

1.2 Problem Definition

In this research the ELV data studied is that of the sixth Atlas-Centaur flight (AC-6). The Surveyor program of lunar probes consisted of several AC flights, of which AC-6 was a test flight with a simulated payload in 1965. AC-6 is representative of current ELV designs with available data that does not have ITAR or company proprietary restrictions [7]-[11]. Figure 1 shows the launch of AC-10, the NASA Surveyor 1 mission that scouted the lunar surface for future Apollo manned lunar landing sites.

Figure 1. Atlas-Centaur 10 - Carrying the Surveyor 1 Spacecraft (NASA)

The goal of this research is to solve an attitude control problem of an AC-6 type ELV during its boost flight by investigating the direct MRAC approach utilizing Lyapunov stability theory. It is followed by testing the control scheme under the presence of environmental and dynamical uncertainties.

1.3 Approach

Indirect methods of adaptive control require plant parameter estimation. The direct approach only estimates controller parameters via adaptive gains that are derived through an adaptation law. The method investigated in this thesis does not rely on convergence of the estimated control parameters to their true unknown values, but are required to be bounded for stability.

The first step will be to use a system plant (e.g. ELV) with known dynamics structure but unknown parameters. Next, a reference system that specifies the desired response to a given

command signal (e.g. pitch rate) is selected. Then the controller is parameterized and an adaptation law that adjusts the parameters based on the state error between the plant and reference model is developed. To guarantee stability, the adaptive law is chosen such that the time-derivative of a chosen Lyapunov function decreases along the error dynamics trajectory [12]. Figure 2 shows the generic architecture of the direct MRAC approach.

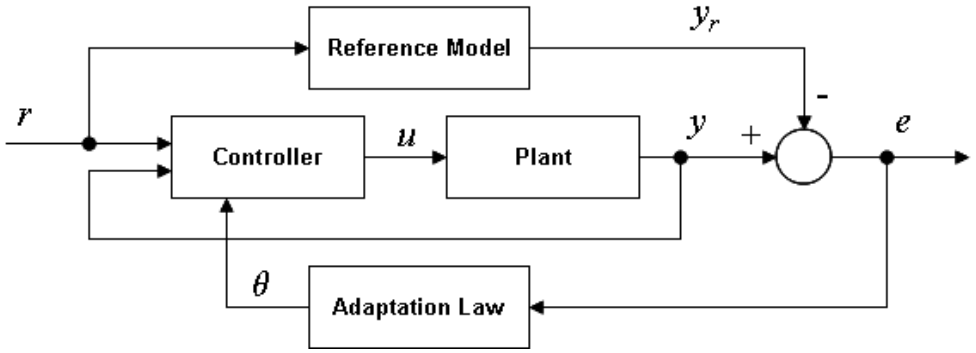

Figure 2. General MRAC Architecture

The baseline Atlas-Centaur controller [10] (i.e. proportional-integral control) is applied because it provided good tracking of the input command (i.e. pitch rate command). To obtain the reference model, Jacobian linearization of the system plant (i.e. baseline controller and ELV dynamics) was done at several time-points along the AC-6 trajectory. Because some of the state derivatives have no equilibrium points as the ELV is accelerating, there would have needed to be some type of "scheduling" of reference models for the entire flight envelope. Figure 3 shows this type of MRAC architecture. Notice that the reference command signal (r) to the autopilot is assumed to be supplied by a guidance system in an outer-loop. Most ELVs fly with an open-loop guidance scheme for first part of atmospheric flight (i.e. a pre-determined pitch rate command) that will minimize aerodynamic loading on the vehicle.

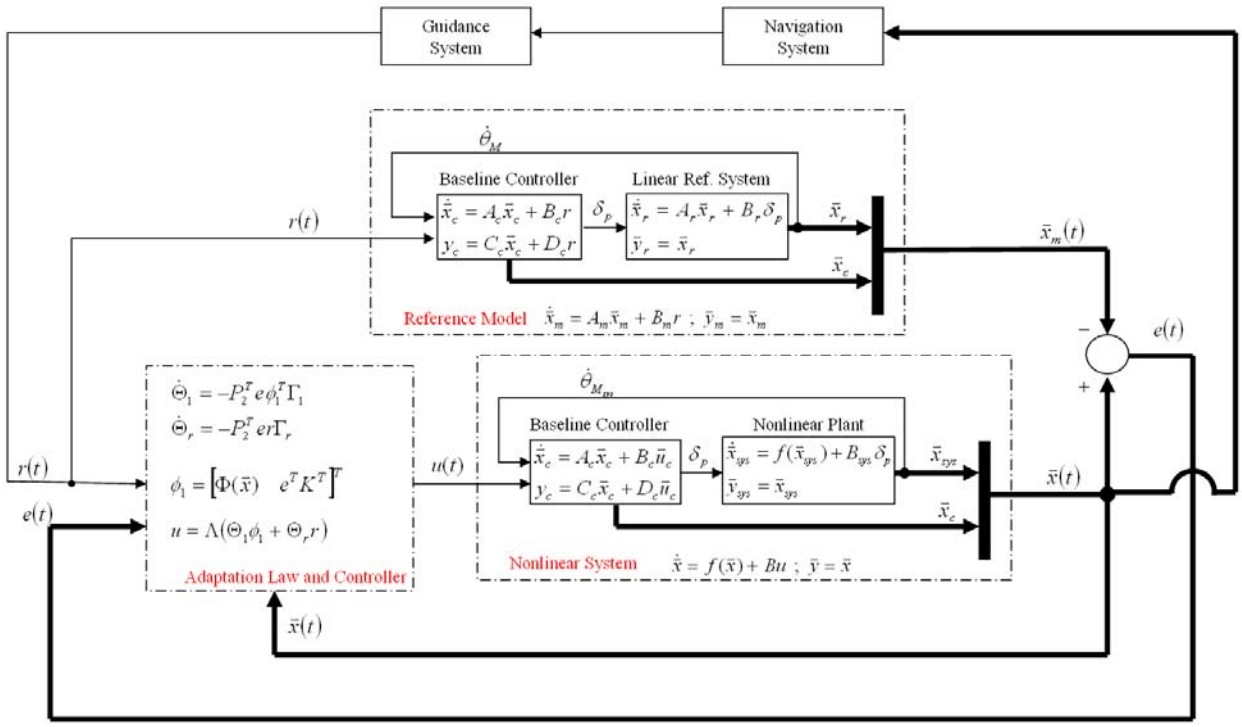

Figure 3. First ELV MRAC Architecture

Feedback linearization methods, and specifically the normal form, of the system dynamics result in a linear time-invariant (LTI) reference model development. The methods of feedback linearization, in [13] and [14], transform the nonlinear system into an equivalent linear system through a change of variables and suitable control input. An LTI reference model can be found of the same order of the transformed nonlinear dynamics. The architecture shown in Figure 4 is what was used in the research presented by this thesis.

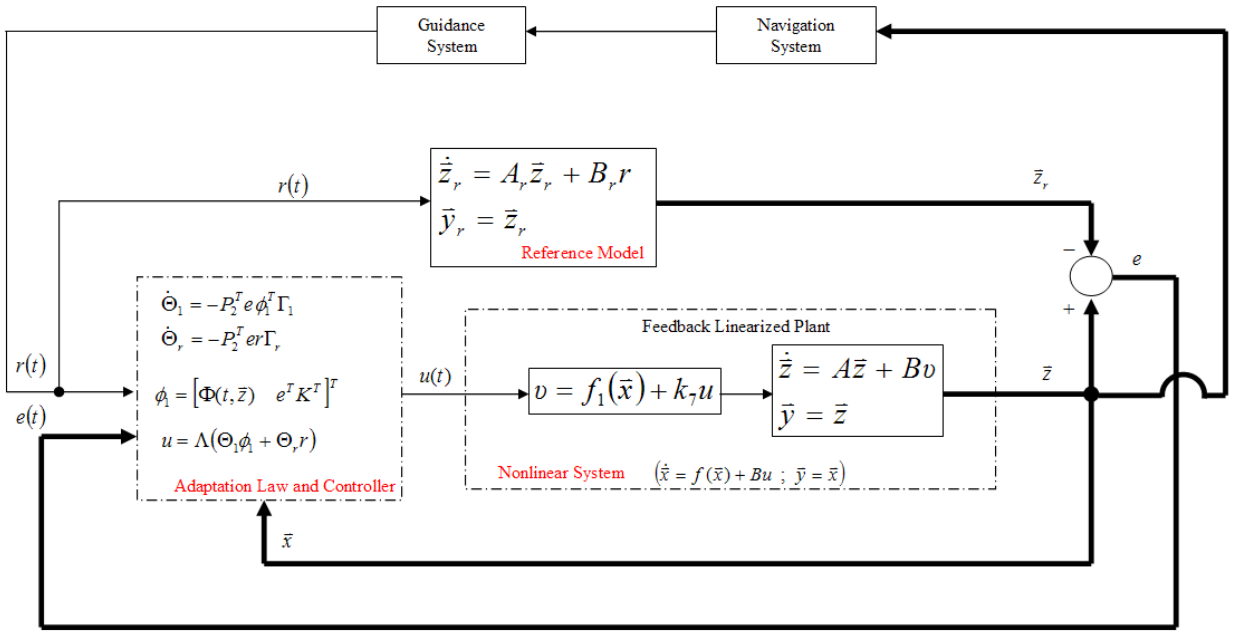

Figure 4. Final ELV MRAC Architecture

1.4 Overview

This document consists of six chapters. In chapter 2 a review of previous work in the field of aerospace adaptive control is done. Chapter 3 derives the equations of motion of the pitch-plane dynamics of the ELV. In chapter 4 the MRAC architecture is derived based on the Lyapunov stability theory found in [12]. Various system simulation results are shown in chapter 5. The thesis ends with chapter 6 that provides the conclusion of the research and recommendations for future work.

CHAPTER 2: LITERATURE REVIEW

2.1 Aerospace Applications

The theory of adaptive control history is well documented, but its success in aerospace applications is varied. In a paper [15] in 1991, MRAC was one of eight advanced control system design techniques that were evaluated for the USAF Advanced Launch System (ALS) program. The techniques represented a cross-section of recent developments in control synthesis at the time. They included: multivariable linear and nonlinear design and analysis methods, frequency weighting approaches, and adaptive schemes.

That paper [15] stated that direct MRAC had several issues that severely limited it as a viable candidate for ALS application. The most important issue they avowed is that persistent excitation requirements could call for cycling of the gimbaled engines, resulting in non-standard and non-optimal guidance trajectories. While guidance system changes would need to be traded with other benefits of MRAC in order to achieve the desired payload objective, persistent excitation (as it pertains to stability) now can be handled with modifications to direct MRAC. Boundedness of controller parameters has been shown by several authors [17]. Details, or proofs, of the authors' concerns where not shown in the ALS paper.

Another paper [16] discusses direct MRAC for several aircraft and weapon systems. All examples used aerodynamic control surfaces vs. the thrust vector control (TVC) for ELVs. Some use dynamic inversion with neural networks as their control scheme. Important assumptions for all the examples are that the reference models must be stable and are developed by a Jacobian linearization of the system dynamics about trajectory equilibrium (trim) points.

They also assume a special linear form of system dynamics, where the adaptive controller is assumed to augment a baseline linear controller.

2.2 ELV Specific Application

Except for at the trivial first time-point (t=0) in a launch, no equilibrium points exist for an ELV. Jacobian linearization to achieve reference models would not work for ELVs. In a paper in 2006 [18] feedback linearization methods were shown to overcome the analytical intractability of a nonlinear air-breathing hypersonic vehicle with coupled engine and aero-elasticity (bending) dynamics. Using the normal form of [13] and [14] results in a transformation of the nonlinear system to an equivalent linear system with a change of variables and a suitable control input.

Leonessa, et al., has shown in [12] a more general MRAC framework. There are no requirements for a stable reference model or the form of the system dynamics (e.g. dynamics can be nonlinear), as long as the model matching conditions, or compatibility relations, for the uncertainty hold. The paper's real benefit is for systems with actuator rate and amplitude saturation, but the general MRAC premise is useful for this thesis. That paper also expressly states, "If the system dynamics is in Normal Form with asymptotically stable internal dynamics, then one can always construct basis functions (uncertainty) and a stabilizable reference model that meet the matching conditions without requiring knowledge of the system dynamics".

CHAPTER 3: EQUATIONS OF MOTION

3.1 Introduction

For simplicity, only the pitch-plane of the ELV motion is studied in this work. The control problem in the context of the short-period dynamics of the vehicle is concerned mainly with ensuring that the ELV responds satisfactorily to input signals in the form of rate or attitude commands. The long-period dynamics are also of concern in ELV motion. The relations between speed and attitude (long-period) and that of angle-of-attack, attitude, and attitude rate (short-period) are not as decoupled as those in aircraft motion. The energy used for stability and performance of the short-period dynamics may result in undesired final speed and position, i.e. the final orbit.

The derived equations are presented with relation to a defined coordinate system. Several assumptions are made that allow for simplification of the equations. The equations of motion of an ELV are complicated by the fact that the vehicle has time-variable mass and inertia. There are also relative motion between various masses within the vehicle and the origin of the body axes, such as fuel sloshing, engine gimbal rotation, and vehicle flexibility. The derivations and assumptions in this research follow those found in [5].

3.2 Coordinate Frame

The assumed pitch-plane coordinate frame is shown in Figure 5. Forces and moments acting on the ELV are shown in dark bold. The launch azimuth is assumed to be directly East.

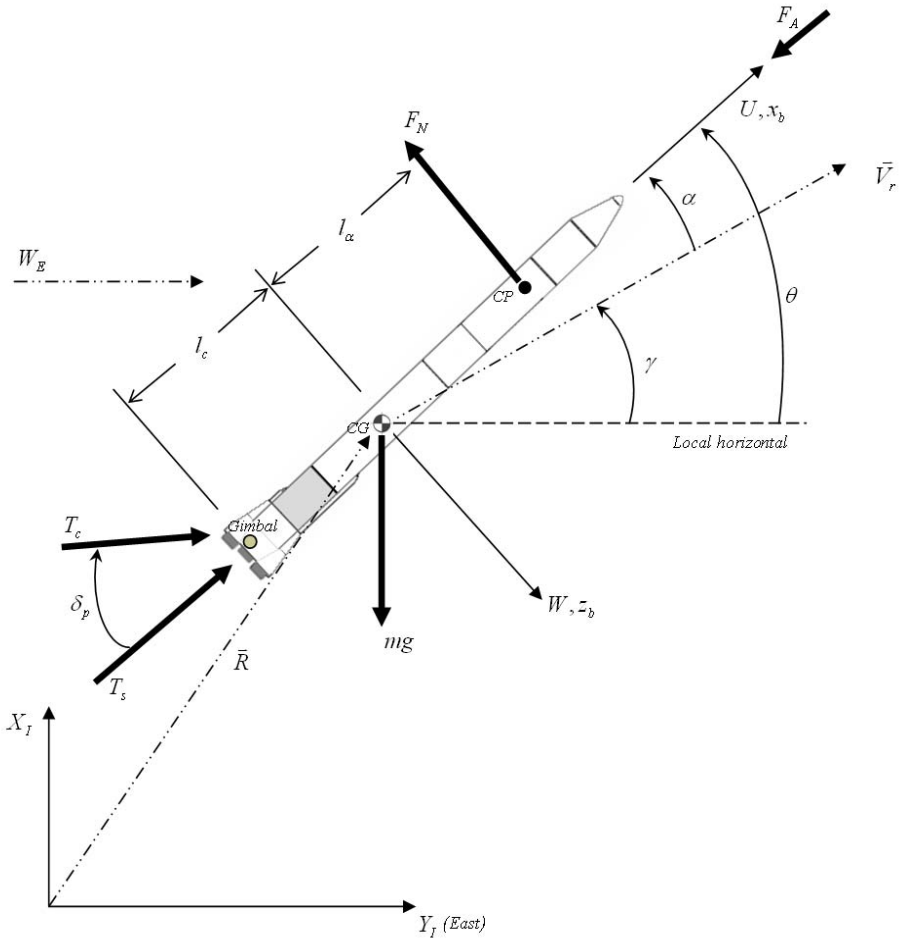

Figure 5. ELV Free-body Diagram of Pitch Plane

Referencing Figure 5 above, the major assumptions are outlined as:

- The inertial origin is at the launch pad on a flat-Earth coordinate frame
- The body axes origin is at the center-of-gravity (CG) of the vehicle
- Only rigid-body motions are considered in the pitch-plane (3-DOF)
- The cross-products of inertia are negligible as the vehicle is symmetric
- Aerodynamic forces are found via look-up tables: $C_A = f(Mach)$ and $C_N = f(\alpha, Mach)$
- Acceleration due to gravity is considered constant (32.174 ft/sec^2)
- Engine deflections are small enough ($\delta_p << 1$) such that $\sin\delta_p \approx \delta_p$ and $\cos\delta_p \approx 1$

- Inertial position, X_I, Y_I, does not affect attitude dynamics directly
- Incidence angle $\alpha << 1$ such that $V_r \approx U$ and $\alpha \approx \left(\frac{W}{U}\right)$

Other useful relationships, including wind velocity W_E, are defined as:

- Relative Airspeed: $V_r = \sqrt{U'^2 + W'^2}$
- Angle-of-Attack: $\alpha = \tan^{-1}\left(\frac{W'}{U'}\right)$
- Flight-Path Angle: $\gamma = \theta - \alpha$
- Dynamic Pressure: $\bar{q} = \frac{1}{2}\rho V_r^2$
- Aerodynamic Forces: $F_A = \bar{q} S_{ref} C_A$ and $F_N = \bar{q} S_{ref}(C_{N_0} + C_{N_\alpha}\alpha)$

The body-axes components of velocity are defined as $U' = U + W_E \cos\theta$ and $W' = W + W_E \sin\theta$.

3.3 Pitch-Plane Equations

The architecture introduced earlier in Figure 3 can be written to separate the baseline controller from the rest of the nonlinear system, where the system dynamics are of the form

$$\begin{aligned} \dot{\vec{x}}_{sys} &= f(\vec{x}_{sys}) + B_{sys}\delta_p \\ \vec{y}_{sys} &= \vec{x}_{sys} \end{aligned} \tag{1}$$

and defined as

$$\begin{bmatrix} \dot{x}_1 \\ \dot{x}_2 \\ \dot{x}_3 \\ \dot{x}_4 \end{bmatrix}_{sys} = \begin{bmatrix} \dot{U} \\ \dot{W} \\ \dot{q} \\ q \end{bmatrix} = \begin{bmatrix} -qW - g\sin\theta - \dfrac{\bar{q}S_{ref}C_A}{m} + \dfrac{(T_s + T_c)}{m} \\ qU + g\cos\theta - \dfrac{\bar{q}S_{ref}(C_{N_0} + C_{N_\alpha}\alpha)}{m} \\ -\dfrac{\dot{I}_{yy}}{I_{yy}}q + \dfrac{\bar{q}S_{ref}l_\alpha(C_{N_0} + C_{N_\alpha}\alpha)}{I_{yy}} \\ \dot{\theta} \end{bmatrix} + \begin{bmatrix} 0 \\ \left(\dfrac{T_c}{m}\right) \\ \left(\dfrac{T_c l_c}{I_{yy}}\right) \\ 0 \end{bmatrix}\delta_p \tag{2}$$

The baseline controller output is defined as

$$\delta_c = \delta_p = c_I + K_A\left(\theta_e - K_R\dot{\theta}\right) \tag{3}$$

Where the baseline controller system dynamics are shown in Figure 6 and defined as

$$\begin{aligned} \dot{\vec{x}}_c &= A_c\vec{x}_c + B_c\vec{u}_c \\ y_c &= C_c\vec{x}_c + D_c\vec{u}_c \end{aligned} \tag{4}$$

or

$$\begin{aligned} \begin{bmatrix} \dot{\theta}_e \\ \dot{c}_I \end{bmatrix} &= \begin{bmatrix} 0 & 0 \\ K_A K_I & 0 \end{bmatrix}\begin{bmatrix} \theta_e \\ c_I \end{bmatrix} + \begin{bmatrix} 1 & -1 \\ 0 & -K_A K_I K_R \end{bmatrix}\begin{bmatrix} \dot{\theta}_c \\ \dot{\theta}_M \end{bmatrix} \\ \delta_c = \delta_p &= \begin{bmatrix} K_A & 1 \end{bmatrix}\begin{bmatrix} \theta_e \\ c_I \end{bmatrix} + \begin{bmatrix} 0 & -K_A K_R \end{bmatrix}\begin{bmatrix} \dot{\theta}_c \\ \dot{\theta}_M \end{bmatrix} \end{aligned} \tag{5}$$

Where K_A and K_I are the baseline controller gains and K_R is the rate gyro gain. The pitch program, $\dot{\theta}_c$, is the commanded (or desired) rate input to the control system and also is the reference signal (r).

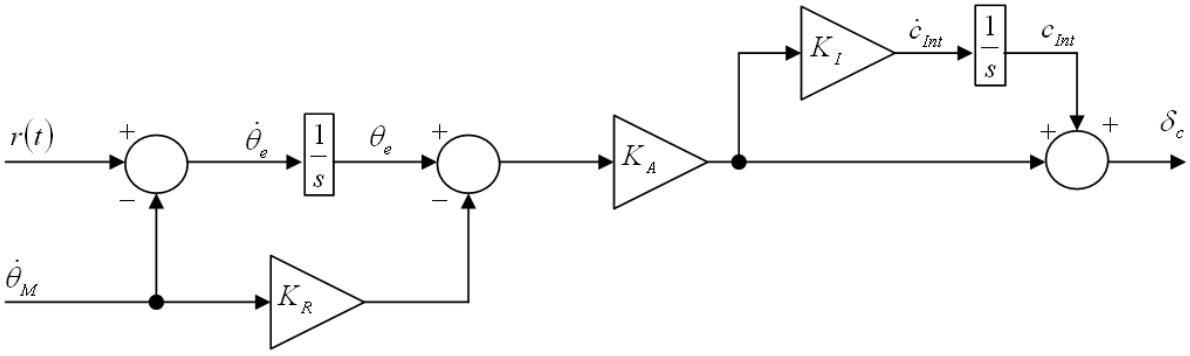

Figure 6. Baseline Control System Block Diagram

The following state variables are defined for the nonlinear system with the baseline controller

$$\vec{x} = \begin{bmatrix} U & W & q & \theta & c_I & \theta_e \end{bmatrix}^T = \begin{bmatrix} x_1 & x_2 & x_3 & x_4 & x_5 & x_6 \end{bmatrix}^T \tag{6}$$

The nonlinear system dynamics can now be put in the form

$$\begin{aligned} \dot{\vec{x}} &= f(\vec{x}) + g(\vec{x})u \\ \vec{y} &= h(\vec{x}) \end{aligned} \tag{7}$$

After substituting for δ_p and the variable definitions, the state equation with no wind becomes

$$\begin{bmatrix} \dot{x}_1 \\ \dot{x}_2 \\ \dot{x}_3 \\ \dot{x}_4 \\ \dot{x}_5 \\ \dot{x}_6 \end{bmatrix} = \begin{bmatrix} -x_3 x_2 - g\sin x_4 - \dfrac{\rho S_{ref} C_A x_1^2}{2m} + \dfrac{(T_s + T_c)}{m} \\ x_3 x_1 + g\cos x_4 - \dfrac{\rho S_{ref}(C_{N_0} x_1^2 + C_{N_\alpha} x_1 x_2)}{2m} + \dfrac{T_c}{m}\left(x_5 + K_A\left(x_6 - x_3 K_R\right)\right) \\ -\dfrac{\dot{I}_{yy}}{I_{yy}} x_3 + \dfrac{\rho S_{ref} l_\alpha (C_{N_0} x_1^2 + C_{N_\alpha} x_1 x_2)}{2I_{yy}} + \dfrac{T_c l_c}{I_{yy}}\left(x_5 + K_A\left(x_6 - x_3 K_R\right)\right) \\ x_3 \\ K_A K_I (x_6 - x_3 K_R) \\ -x_3 \end{bmatrix} + \begin{bmatrix} 0 \\ 0 \\ 0 \\ 0 \\ 0 \\ 1 \end{bmatrix} u \tag{8}$$

The output equation is chosen as $\vec{y} = x_4 = \theta$. It is also convenient to define other parameters in (8) as constants, then the nonlinear equation becomes

$$\begin{bmatrix} \dot{x}_1 \\ \dot{x}_2 \\ \dot{x}_3 \\ \dot{x}_4 \\ \dot{x}_5 \\ \dot{x}_6 \end{bmatrix} = \begin{bmatrix} -x_3 x_2 - K_1 \sin x_4 - C_1 x_1^2 + K_2 \\ x_3 x_1 + K_1 \cos x_4 - C_2 x_1^2 - C_3 x_1 x_2 + K_3 x_5 + K_4 x_6 - K_5 x_3 \\ -K_{11} x_3 - K_8 x_3 + C_4 x_1^2 + C_5 x_1 x_2 + K_6 x_5 + K_7 x_6 \\ x_3 \\ -K_9 x_3 + K_{10} x_6 \\ -x_3 \end{bmatrix} + \begin{bmatrix} 0 \\ 0 \\ 0 \\ 0 \\ 0 \\ 1 \end{bmatrix} u \tag{9}$$

Where the constants are defined as

$$K_1 = g \qquad C_1 = \frac{\rho S_{ref} C_A}{2m}$$

$$K_2 = \frac{T_s + T_c}{m} \qquad C_2 = \frac{\rho S_{ref} C_{N_0}}{2m}$$

$$K_3 = \frac{T_c}{m} \qquad C_3 = \frac{\rho S_{ref} C_{N_\alpha}}{2m}$$

$$K_4 = \frac{T_c K_A}{m} \qquad C_4 = \frac{\rho S_{ref} l_\alpha C_{N_0}}{2I_{yy}}$$

$$K_5 = \frac{T_c K_A K_R}{m} \qquad C_5 = \frac{\rho S_{ref} l_\alpha C_{N_\alpha}}{2I_{yy}}$$

$$K_6 = \frac{T_c l_c}{I_{yy}}$$

$$K_7 = \frac{T_c l_c K_A}{I_{yy}}$$

$$K_8 = \frac{T_c l_c K_A K_R}{I_{yy}}$$

$$K_9 = K_A K_I K_R$$

$$K_{10} = K_A K_I$$

$$K_{11} = \frac{\dot{I}_{yy}}{I_{yy}}$$

3.4 Summary

The equations of motion of (9) are now in a form that is convenient for feedback linearization and adaptive control design. The next chapter will show the derivation of the reference model and adaptive controller.

CHAPTER 4: CONTROL SYSTEM DESIGN

4.1 Introduction

In order to obtain the adaptive control architecture defined in Figure 4, feedback linearization will be performed on the nonlinear system dynamics. This will transform the nonlinear system into an equivalent linear system through a change of variables and suitable control input. A special notation is introduced, called the Lie derivative [14] that is convenient for taking multiple derivatives with respect to the same (or different) vector field. A reference model can then be developed that meets the compatibility relations.

4.2 Feedback Linearization

To obtain the normal form of the feedback linearized system, one takes the time-derivative of the output in successive instances until the input variable appears in the equation. If the nonlinear equations are in the form

$$\begin{aligned} \dot{x} &= f(x) + g(x)u \\ y &= h(x) \end{aligned} \tag{10}$$

Where $x \in \Re^n$ is the state vector, $u \in \Re^p$ is the vector of inputs, and $y \in \Re^m$ is the vector of outputs. The first time-derivative of the output in (10) is

$$\dot{y} = \frac{\partial h(x)}{\partial x}\dot{x} = \frac{\partial h(x)}{\partial x}\left(f(x) + g(x)u\right) \tag{11}$$

The time derivative of the output equation in terms of Lie derivatives is

$$\dot{y} = L_f h(x) + L_g h(x)u \tag{12}$$

Where the definition of the Lie derivative of $h(x)$ with respect to $f(x)$ is $L_f h(x) = \frac{\partial h(x)}{\partial x} f(x)$ and the Lie derivative of $h(x)$ with respect to $g(x)$ is $L_g h(x) = \frac{\partial h(x)}{\partial x} g(x)$.

The relative degree (r_d) of the system can be considered as the number of times the output (y) needs to be differentiated before the input (u) appears in the equation. Assuming $r_d = n$, then

$$\begin{aligned} y &= h(x) \\ \dot{y} &= L_f h(x) \\ \ddot{y} &= L_f^2 h(x) \\ &\vdots \\ y^{(n)} &= L_f^n h(x) + L_g L_f^{n-1} h(x) u \end{aligned} \tag{13}$$

The state transformation can now be expressed in a new state vector z as

$$\begin{bmatrix} z_1(x) \\ z_2(x) \\ \vdots \\ z_n(x) \end{bmatrix} = \begin{bmatrix} h(x) \\ L_f h(x) \\ \vdots \\ L_f^{n-1} h(x) \end{bmatrix} \tag{14}$$

and the resulting system is then effectively a bank of n integrators

$$\begin{bmatrix} \dot{z}_1(x) \\ \dot{z}_2(x) \\ \vdots \\ \dot{z}_n(x) \end{bmatrix} = \begin{bmatrix} L_f h(x) \\ L_f^2 h(x) \\ \vdots \\ L_f^n h(x) + L_g L_f^{n-1} h(x) u \end{bmatrix} = \begin{bmatrix} z_2 \\ z_3 \\ \vdots \\ \upsilon \end{bmatrix} \tag{15}$$

4.2.1 ELV Formulation

For the ELV system dynamics in (9), recall the chosen output is $y = x_4 = \theta$ and successive time differentiations result in

$$\begin{aligned}
\dot{y} &= \dot{x}_4 = \dot{\theta} = x_3 \\
\ddot{y} &= \ddot{x}_4 = \ddot{\theta} = \dot{x}_3 = -(K_8 + K_{11})x_3 + C_4 x_1^2 + C_5 x_1 x_2 + K_6 x_5 + K_7 x_6 \\
\dddot{y} &= \dddot{x}_4 = \dddot{\theta} = \ddot{x}_3 = -(K_8 + K_{11})\dot{x}_3 + C_4 x_1 \dot{x}_1 + C_5(\dot{x}_1 x_2 + x_1 \dot{x}_2) + K_6 \dot{x}_5 + K_7 \dot{x}_6
\end{aligned}$$

or
$$\dddot{y} = f_1(x) + K_7 u \tag{16}$$

where

$$\begin{aligned}
f_1(x) = &-(2C_1C_4 + C_2C_5)x_1^3 - (K_8 + K_{11})C_4 x_1^2 - (C_1C_5 + C_3C_5)x_1^2 x_2 + C_5 x_1^2 x_3 - 2C_4 x_1 x_2 x_3 \\
&- (K_8 + K_{11})C_5 x_1 x_2 - C_5 K_5 x_1 x_3 + C_5 K_3 x_1 x_5 + C_5 K_4 x_1 x_6 + 2C_4 K_2 x_1 - 2C_4 K_1 x_1 \sin x_4 \\
&- C_5 K_1 x_1 \cos x_4 - C_5 x_2^2 x_3 + C_5 K_2 x_2 - C_4 K_1 x_2 \sin x_4 + \left[(K_8 + K_{11})^2 - K_6 K_9 - K_7\right]x_3 \\
&- (K_8 + K_{11})K_6 x_5 + \left[K_6 K_{10} - (K_8 + K_{11})K_7\right]x_6
\end{aligned}$$

The transformed system dynamics in the normal form of Figure 4 is then

$$\begin{bmatrix} \dot{z}_1(x) \\ \dot{z}_2(x) \\ \dot{z}_3(x) \end{bmatrix} = \begin{bmatrix} z_2 \\ z_3 \\ \upsilon \end{bmatrix} = \begin{bmatrix} \dot{\theta} \\ \ddot{\theta} \\ f_1(x) + K_7 u \end{bmatrix} = \begin{bmatrix} q \\ \dot{q} \\ f_1(x) + K_7 u \end{bmatrix} \tag{17}$$

4.2.2 Reference Model

The reference model is chosen such that it tracks the reference signal (r) sufficiently and has the same number of transformed states (z) as the feedback linearized ELV system. It is desired for the reference model to respond to the commanded pitch rate reference signal sufficiently, i.e. the rise and settling times should be approximately 0.6 sec and 2 sec respectively, and a peak overshoot of less than 15%. A second order

system with damping of 0.53 and frequency of 2.83 rad/sec achieves the desired pitch rate response to a reference step input (see Figure 7). The transfer function representation is

$$\frac{z_2(s)}{r(s)} = \frac{8}{s^2 + 3s + 8}$$

Where the second order systems for angular position and acceleration would then be

$$\frac{z_1(s)}{r(s)} = \frac{8}{s^3 + 3s^2 + 8s}$$

$$\frac{z_3(s)}{r(s)} = \frac{8s}{s^2 + 3s + 8}$$

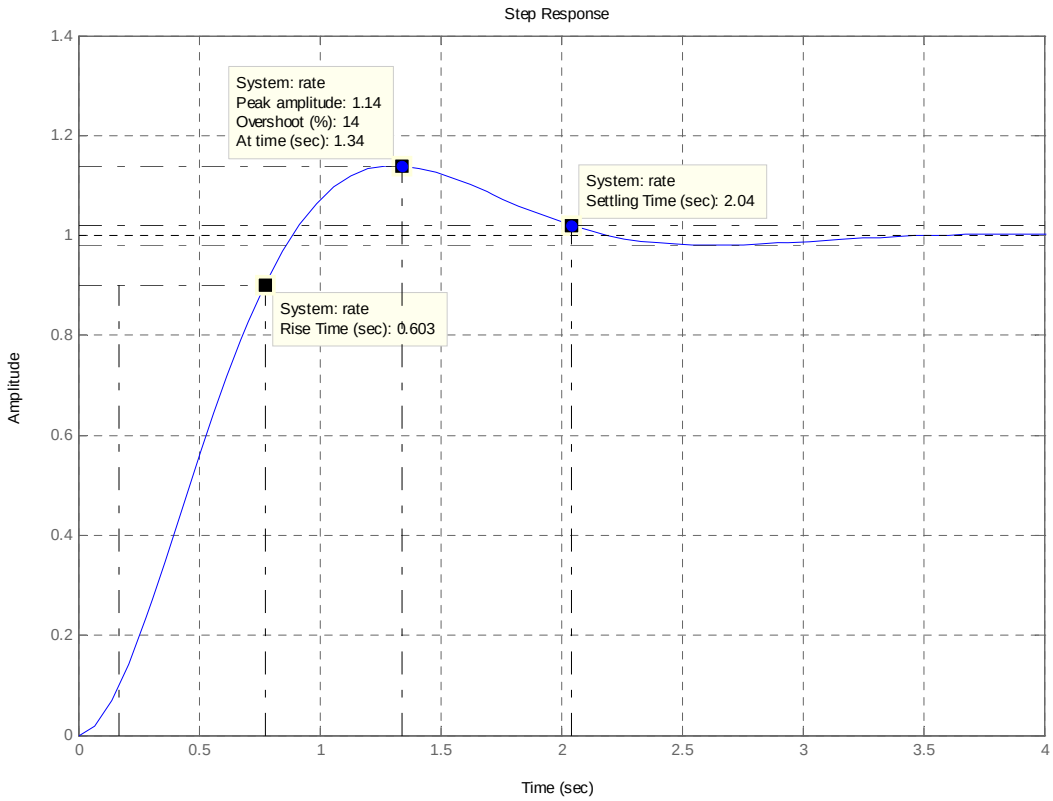

Figure 7. Rate Output Step Response of Selected Reference Model

The multiple output reference model in control canonical form then becomes

$$\begin{aligned} \dot{z}_r &= A_r z_r + B_r r \\ y_r &= C_r z_r + D_r r \end{aligned} \tag{18}$$

or

$$\begin{aligned} \begin{bmatrix} \dot{z}_1 \\ \dot{z}_2 \\ \dot{z}_3 \end{bmatrix} &= \begin{bmatrix} 0 & 1 & 0 \\ 0 & 0 & 1 \\ 0 & -8 & -3 \end{bmatrix} \begin{bmatrix} z_1 \\ z_2 \\ z_3 \end{bmatrix} + \begin{bmatrix} 0 \\ 0 \\ 8 \end{bmatrix} r \\ y_r &= \begin{bmatrix} 1 & 0 & 0 \\ 0 & 1 & 0 \\ 0 & 0 & 1 \end{bmatrix} \begin{bmatrix} z_1 \\ z_2 \\ z_3 \end{bmatrix} + \begin{bmatrix} 0 \\ 0 \\ 0 \end{bmatrix} r \end{aligned} \tag{19}$$

4.3 MRAC Design

With the nonlinear system dynamics given in (9) and the reference model of (19), the adaptive controller can now be derived. To characterize the adaptive feedback tracking control law for a nonlinear uncertain system, consider the ELV equations derived in (17) as

$$\dot{z}(t) = f(z(t)) + Bu(t), \quad z(0) = z_0, \quad t \geq 0 \tag{20}$$

Where $z \in \Re^{n_z}$ is the state vector and $u \in \Re^m$ is the vector of inputs. Using the notation found in [12], assuming a desired trajectory is given as $z_d(t),\ t \geq 0$, the objective is to find a $u(t),\ t \geq 0$ so that the system tracks the desired trajectory (i.e. $\lim_{t\to\infty} \|z(t) - z_d(t)\| = 0$). Recall that in (19) the reference trajectory need not be stable, only that $A_r \in \Re^{n_z \times n_z}$ and $B_r \in \Re^{n_z \times m}$ such that the pair (A_r, B_r) is stabilizable (i.e. all unstable modes are controllable).

Restated, the goal is to design $u(t),\ t \geq 0$ and a bounded piecewise continuous reference function $r(t),\ t \geq 0$, such that

$$\lim_{t\to\infty}\|z(t)-z_r(t)\|=0 \quad \Rightarrow \quad \lim_{t\to\infty}\|z_r(t)-z_d(t)\|=0 \quad \Rightarrow \quad \lim_{t\to\infty}\|z(t)-z_d(t)\|=0 \tag{21}$$

When the system dynamics are known, the tracking error can be defined as

$$e(t)=z(t)-z_r(t) \qquad e(0)=z_0-z_{r_0}=e_0 \tag{22}$$

With the error dynamics defined as

$$\dot{e}(t)=\dot{z}(t)-\dot{z}_r(t)=\{f(z(t))+Bu(t)\}-\{A_r z_r(t)+B_r r(t)\} \tag{23}$$

Theorem 2.1 of [12] assumes that ideal gain matrices $\Theta^* \in \Re^{m\times s}$ and $\Theta_r^* \in \Re^{m\times m}$ exist, as well as function $\Phi : \Re^n \to \Re^s$ such that the compatibility equations are

$$\begin{aligned} 0 &= f(z)+B\Theta^*\Phi(x)-A_r z \qquad\qquad x\in\Re^n \\ 0 &= B\Theta_r^*-B_r \end{aligned} \tag{24}$$

For the ELV system dynamics, (24) becomes

$$\begin{aligned} \begin{bmatrix}0\\0\\0\end{bmatrix} &= \begin{bmatrix}z_2\\z_3\\f_1(x)\end{bmatrix}+\begin{bmatrix}0\\0\\K_7\end{bmatrix}\Theta^*\Phi(x)-\begin{bmatrix}0&1&0\\0&0&1\\0&-8&-3\end{bmatrix}\begin{bmatrix}z_1\\z_2\\z_3\end{bmatrix} \\ \begin{bmatrix}0\\0\\0\end{bmatrix} &= \begin{bmatrix}0\\0\\K_7\end{bmatrix}\Theta_r^*-\begin{bmatrix}0\\0\\8\end{bmatrix} \end{aligned} \tag{25}$$

In order for (25) to hold, the ideal gain matrices must cancel with the uncertainty in the last rows of both equations.

Even though there is no stability requirement on the reference model, it still must be stabilizible. To deal with unstable reference models, let there be a gain $K \in \Re^{m \times n_z}$ that is defined by

$$K = -R_2^{-1} B_r^T P \tag{26}$$

Where the $n_z \times n_z$ positive definite matrix P satisfies the algebraic Riccati equation

$$0 = A_r^T P + P A_r - P B_r R_2^{-1} B_r^T P + R_1 \tag{27}$$

The arbitrary positive definite matrices that are designed to stabilize the system are $R_1 \in \Re^{n_z \times n_z}$ and $R_2 \in \Re^{m \times m}$. The control law then becomes

$$u(t) = \Theta_1^* \Phi_1(t) + \Theta_r^* r(t) \tag{28}$$

where

$$\begin{aligned} \Theta_1^* &= \begin{bmatrix} \Theta^* & \Theta_r^* \end{bmatrix} \in \Re^{m \times (s+m)} \\ \Phi_1 &= \begin{bmatrix} \Phi^T(x) & e^T K^T \end{bmatrix} \in \Re^{s+m} \end{aligned} \tag{29}$$

When the ideal gains are not known, only that they exist such that the compatibility equations (25) hold, the goal is to construct the estimates $\Theta(t) \in \Re^{m \times s}$ and $\Theta_r(t) \in \Re^{m \times m}$. Using the same gain K defined in (26), P can be partitioned such that

$$P = \begin{bmatrix} P_1 & P_2 \end{bmatrix} > 0 \qquad \begin{aligned} P_1 &\in \Re^{n_z \times (n_z - m)} \\ P_2 &\in \Re^{n_z \times m} \end{aligned} \tag{30}$$

The ELV control now becomes

$$u(t) = \Theta_1(t)\Phi_1(t) + \Theta_r(t)r(t) \tag{31}$$

With adaptive design parameters defined as Γ_1 and Γ_r, the adaptation laws are

$$\begin{aligned} \dot{\Theta}_1(t) &= -P_2^T e(t)\Phi_1^T(t)\Gamma_1 \qquad \Theta_1(0) = 0 \qquad \Gamma_1 \in \Re^{(s+m)\times(s+m)} \\ \dot{\Theta}_r(t) &= -P_2^T e(t)r^T(t)\Gamma_r \qquad \Theta_r(0) = 0 \qquad \Gamma_r \in \Re^{m\times m} \end{aligned} \tag{32}$$

Proof that $e(t) \to 0$ as $t \to \infty$ can be found in [12].

4.4 Basis Functions

With the adaptive controller defined by (32), basis functions must be derived that attempt to approximate the uncertainty in the system. Recall from (16) that

$$\begin{aligned} f_1(x) = &-(2C_1C_4 + C_2C_5)x_1^3 - (K_8 + K_{11})C_4x_1^2 - (C_1C_5 + C_3C_5)x_1^2x_2 + C_5x_1^2x_3 - 2C_4x_1x_2x_3 \\ &- (K_8 + K_{11})C_5x_1x_2 - C_5K_5x_1x_3 + C_5K_3x_1x_5 + C_5K_4x_1x_6 + 2C_4K_2x_1 - 2C_4K_1x_1\sin x_4 \\ &- C_5K_1x_1\cos x_4 - C_5x_2^2x_3 + C_5K_2x_2 - C_4K_1x_2\sin x_4 + \left[(K_8 + K_{11})^2 - K_6K_9 - K_7\right]x_3 \\ &- (K_8 + K_{11})K_6x_5 + \left[K_6K_{10} - (K_8 + K_{11})K_7\right]x_6 \end{aligned} \tag{33}$$

If all the ELV states (x) can be measured then the basis function can be chosen from (33) as

$$\begin{aligned} \Phi(x) = \big[&x_3 \quad x_1x_3 \quad x_1x_2x_3 \quad x_1^2x_3 \quad x_2^2x_3 \quad x_1\sin x_4 \quad x_1\cos x_4 \quad x_2\sin x_4 \quad x_1 \quad \cdots \\ &x_2 \quad x_5 \quad x_6 \quad x_1x_2 \quad x_1x_5 \quad x_1x_6 \quad x_1^2 \quad x_1^2x_2 \quad x_1^3\big]^T \end{aligned} \tag{34}$$

Where the control parameter estimates are defined as

$$\begin{aligned} \Theta = \big[&\theta_1 \quad \theta_2 \quad \theta_3 \quad \theta_4 \quad \theta_5 \quad \theta_6 \quad \theta_7 \quad \theta_8 \quad \theta_9 \quad \cdots \\ &\theta_{10} \quad \theta_{11} \quad \theta_{12} \quad \theta_{13} \quad \theta_{14} \quad \theta_{15} \quad \theta_{16} \quad \theta_{17} \quad \theta_{18}\big] \end{aligned} \tag{35}$$

Then (29) becomes

$$\begin{aligned}\Theta_1 &= \begin{bmatrix}\Theta & \Theta_r\end{bmatrix} \in \Re^{m\times(s+m)} \\ \Phi_1 &= \begin{bmatrix}\Phi^T(x) & e^T K^T\end{bmatrix} \in \Re^{s+m}\end{aligned} \tag{36}$$

When the feedback linearization was performed, two new states (z) had the same physical meaning as two of the previous states (x). Because

$$\begin{bmatrix} z_1 \\ z_2 \end{bmatrix} = \begin{bmatrix} \theta \\ \dot{\theta} \end{bmatrix} = \begin{bmatrix} x_4 \\ x_3 \end{bmatrix} \tag{37}$$

Combining terms in $\Phi(x)$ as a function of x_3 and x_4 results in the ability of the internal dynamics to be approximated by only functions of time,

$$\begin{aligned}\left(x_1^2 + x_1x_2 + x_1 + x_2^2\right)x_3 &\approx \left(\sum_{i=0}^{N} \beta_{1_i} t^i\right) z_2 \\ \left(x_1 + x_2\right)\sin x_4 &\approx \left(\sum_{i=0}^{N} \beta_{2_i} t^i\right)\sin z_1 \\ \left(x_1\right)\cos x_4 &\approx \left(\sum_{i=0}^{N} \beta_{3_i} t^i\right)\cos z_1 \\ f\left(x_1, x_2, x_5, x_6\right) &\approx \left(\sum_{i=0}^{N} \beta_{4_i} t^i\right)\end{aligned}$$

If all of the transformed states (z) can be measured (i.e. angular attitude, angular rate, and angular acceleration), the basis function can then be chosen as a function of time and the new state (z)

$$\begin{aligned}\Phi(t,z) = \Big[&z_2 \quad tz_2 \quad t^2z_2 \quad t^3z_2 \quad t\sin z_1 \quad t^2\sin z_1 \quad t^3\sin z_1 \quad t^4\sin z_1 \quad t\cos z_1 \quad \cdots \\ &t^2\cos z_1 \quad t^3\cos z_1 \quad t^4\cos z_1 \quad t \quad t^2 \quad t^3 \quad t^4 \quad t^4z_2 \quad z_2^3\Big]^T\end{aligned} \tag{38}$$

4.5 Summary

The reference model (19), adaptive control laws (33), and two sets of basis functions (34) and (38) were developed in this chapter. Depending on the measured states that are physically available, either choice of basis function will work. While a 4th order polynomial was implemented to approximate the internal dynamics as functions of only time, any suitable function of time could be used.

The next chapter will show some of the simulation results for both the baseline controller alone and the adaptive controller. Figure 8 shows the overall simulation architecture, which was done in MatLab/Simulink software, with both sets of states fed back to the controller. A switch in the controller can allow either basis function to be used separately in the simulations.

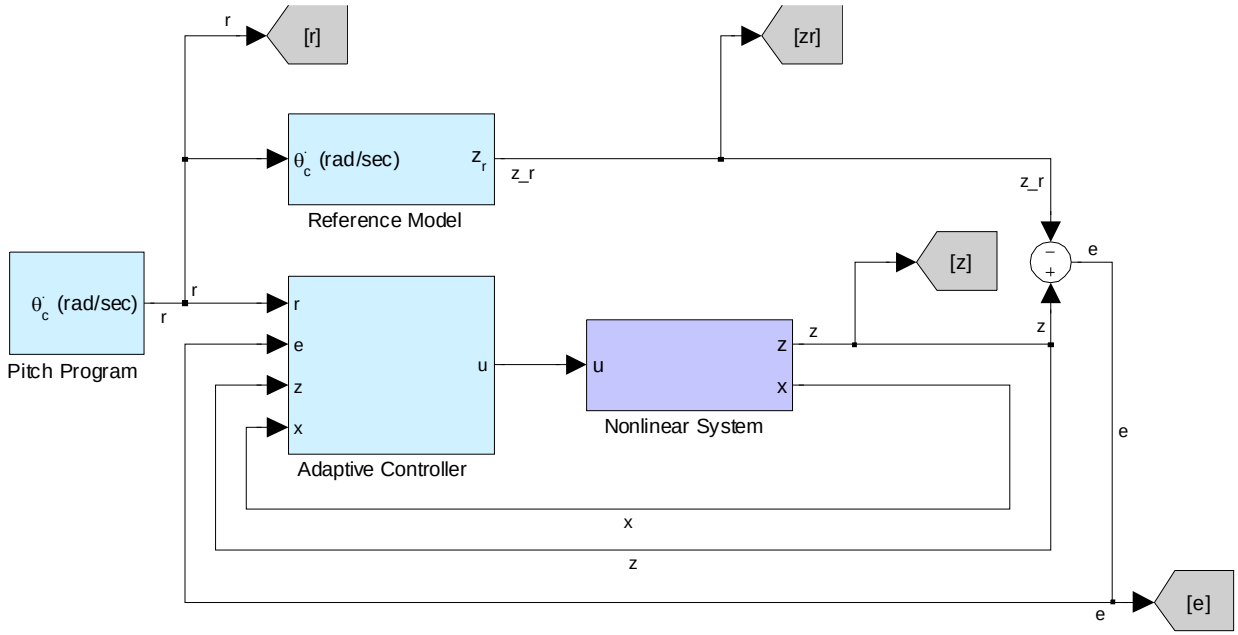

Figure 8. Adaptive Control Architecture Block Diagram

CHAPTER 5: SIMULATION

5.1 Introduction

Several simulation runs were made to validate the baseline controller design, to test the adaptive controller with two sets of basis functions, and to introduce perturbations from nominal ELV parameters. This chapter will outline those simulation results and compare the various test cases. For full flight realization, achievable energy at the end of the boost stage was compared to a percentage of that of the nominal AC-6 flight. This was done to ensure a reasonable energy state at the second stage ignition. It is conservatively assumed that if the energy is within the stated range from AC-6 the upper stage could compensate for the difference and achieve the desired final orbit. The first simulation runs were made with just the nominal nonlinear system with the baseline controller (see Figure 9). Actuator dynamics were neglected in all simulations.

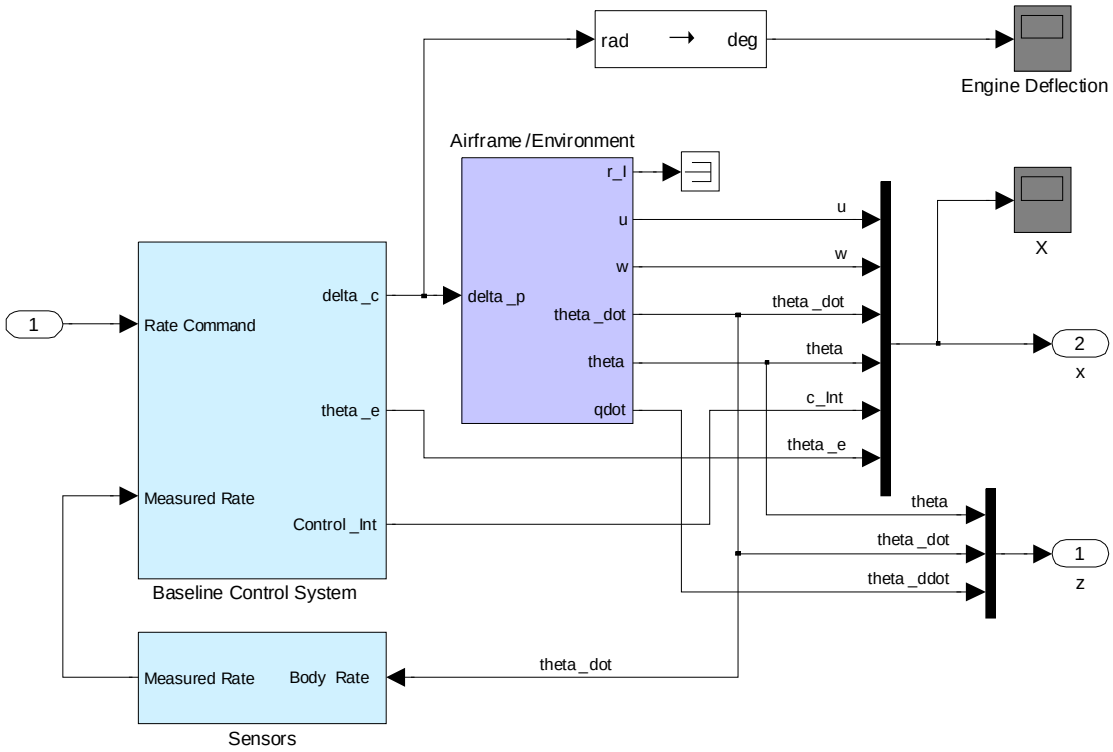

Figure 9. Simulation Overview with Baseline Controller Only

5.2 Baseline Controller Results

Trajectory results with just baseline control used the nominal AC-6 wind profile. The boost phase of flight is defined as launch time (t=0) until Booster Engine Cut-Off (BECO) at 141.88 sec. The baseline controller gains were defined in [10] and set to

$$\begin{aligned} K_A &= 2 \\ K_I &= 0.2 \\ K_R &= 0.485 \end{aligned} \tag{39}$$

The simulation was run until BECO and the values shown in Table 1 were recorded. Negative differences in altitude and speed indicate values less than those found at AC-6 BECO. Negative values in energy indicate there was not enough energy to reach the same altitude and speed as AC-6. Trajectory information is saved during the simulation to evaluate the baseline control system. Figure 10 and Figure 11 show comparisons of the simulated and AC-6 trajectory atmospheric related parameters. Both show that the atmospheric model of the ELV simulation is sufficient for this study.

Table 1. Simulation Values at BECO (Baseline Control Only)

Parameter	ELV Simulation	AC-6 Trajectory	Difference
Altitude (ft)	192,149.50	193,784.50	1,635
Speed (ft/sec)	8254.61	8245.66	-8.95
Energy (%) [desire ± 0.2%]			0.0984

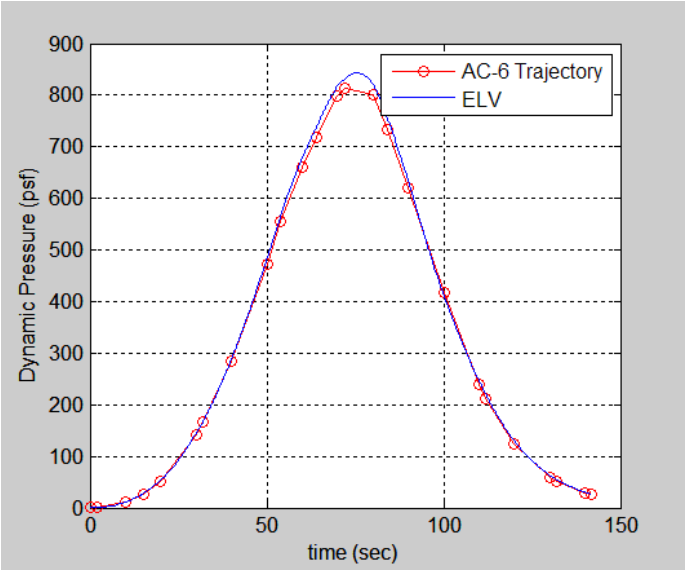

Figure 10. Dynamic Pressure Comparison (Baseline Controller)

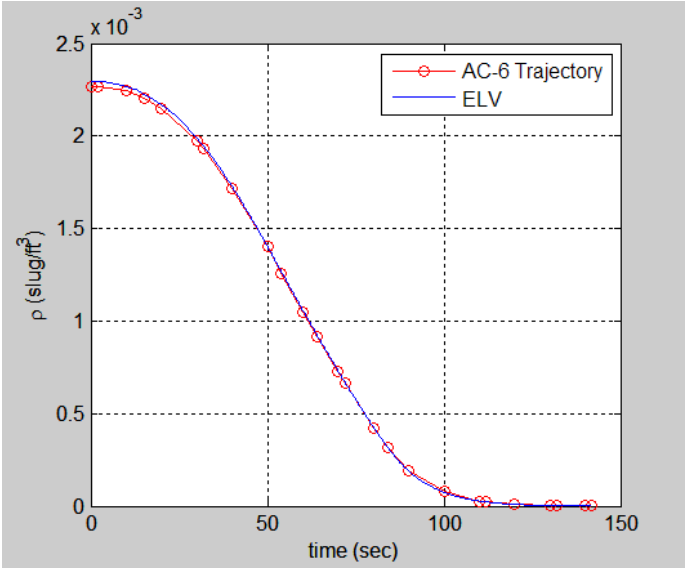

Figure 11. Atmospheric Density Comparison (Baseline Controller)

Next the angle-of-attack and engine deflections where compared. Figure 12 and Figure 13 show these two comparisons. Notice that because the of the assumptions in chapter 3, and the fact that the actual autopilot that flew on AC-6 is not exactly like that found in [10], the engine

deflections are different. But because they are of the same order for peak-to-peak amplitudes, the controller is not commanding unreasonable engine deflections for TVC.

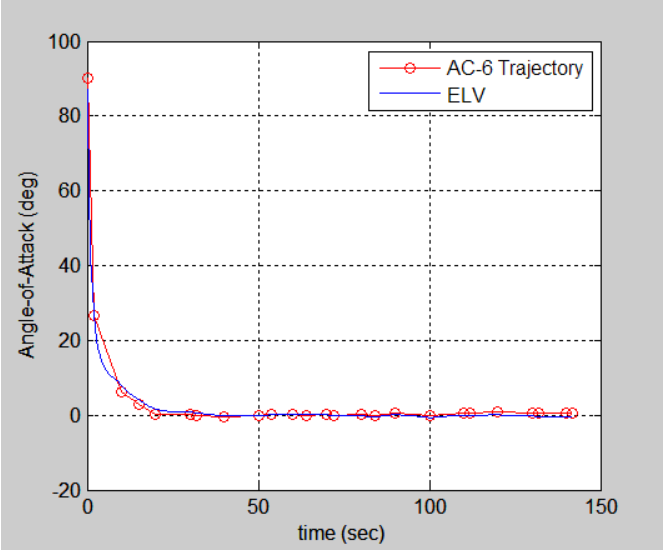

Figure 12. Angle-of-Attack Comparison (Baseline Controller)

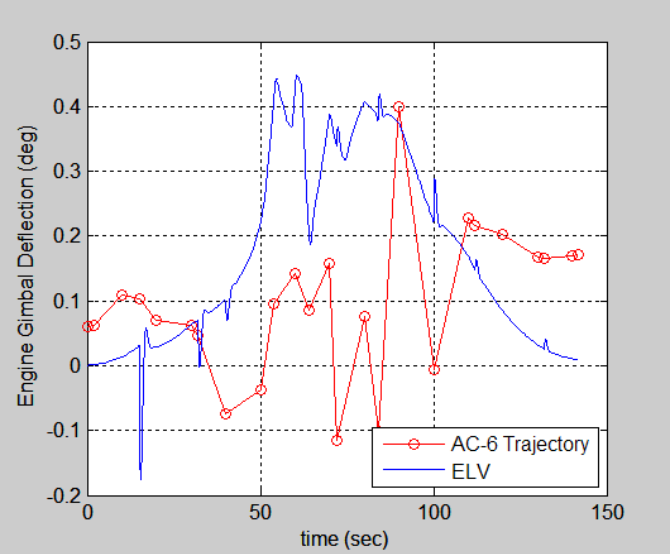

Figure 13. Engine Deflection Comparison (Baseline Controller)

Figure 14 and Figure 15 compare the altitude and speed respectively along the boost trajectory.

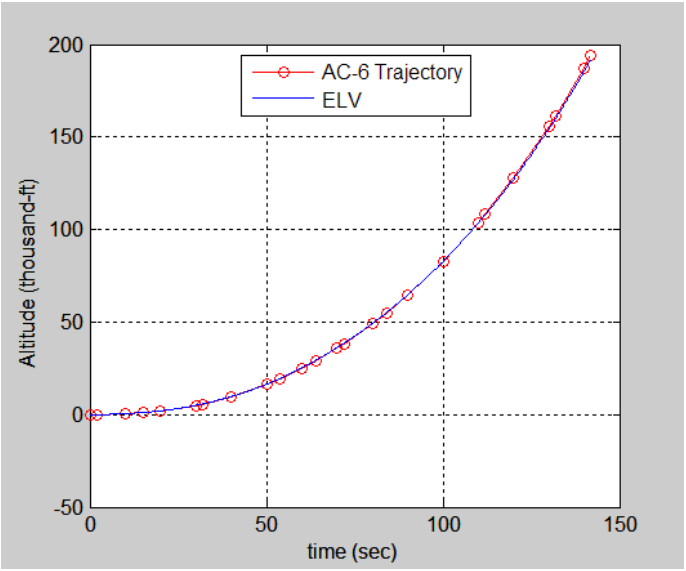

Figure 14. Altitude Comparison (Baseline Controller)

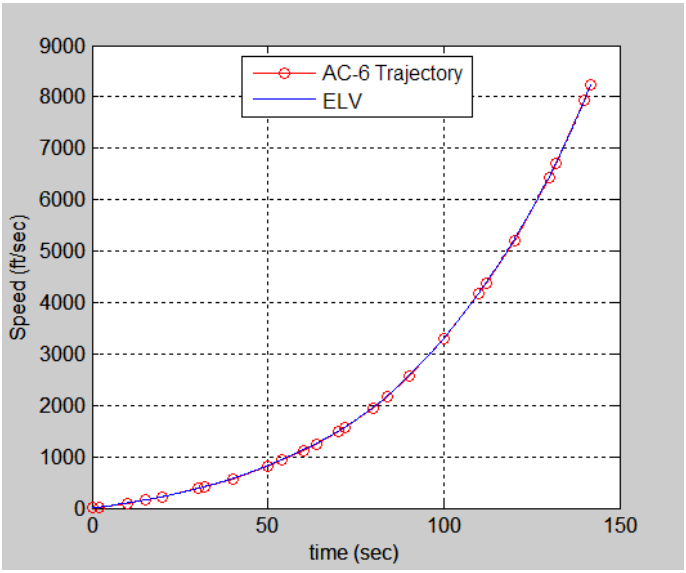

Figure 15. Speed Comparison (Baseline Controller)

The next three figures compare the pitch angular attitude, rate, and acceleration. Notice that in Figure 17 the rate response around the maximum dynamic pressure (t=72 sec) there are variations where the baseline controller cannot track the commanded rate. Also plotted in these

figures are the responses of the reference model (19), to measure the adequacy of its response to the same rate command.

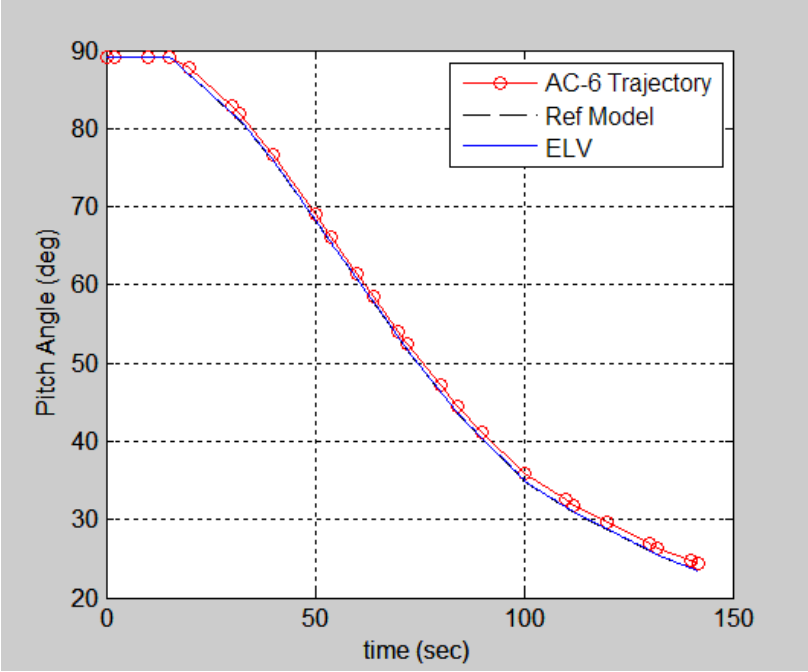

Figure 16. Pitch Attitude Comparison (Baseline Controller)

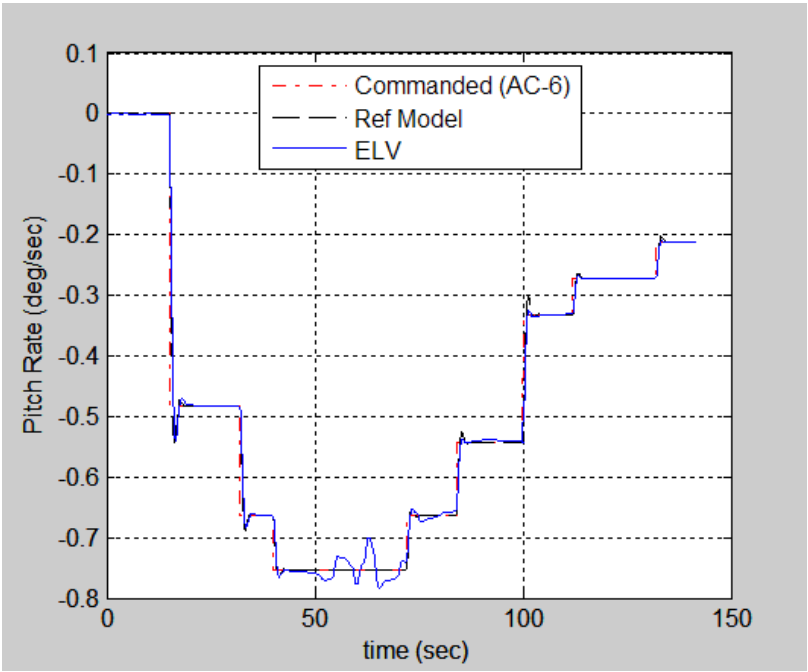

Figure 17. Pitch Angular Rate Comparison (Baseline Controller)

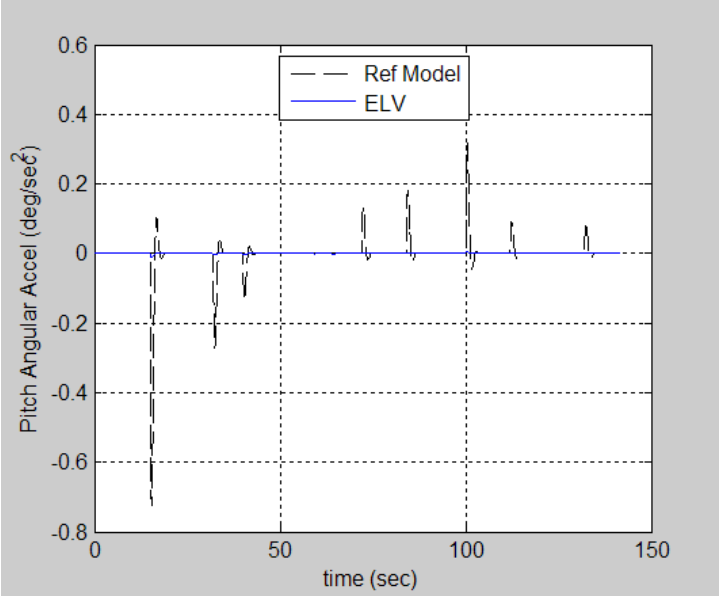

Figure 18. Pitch Angular Acceleration Comparison (Baseline Controller)

Figure 19 shows the error between the chosen reference model states and those in the simulation with the baseline controller.

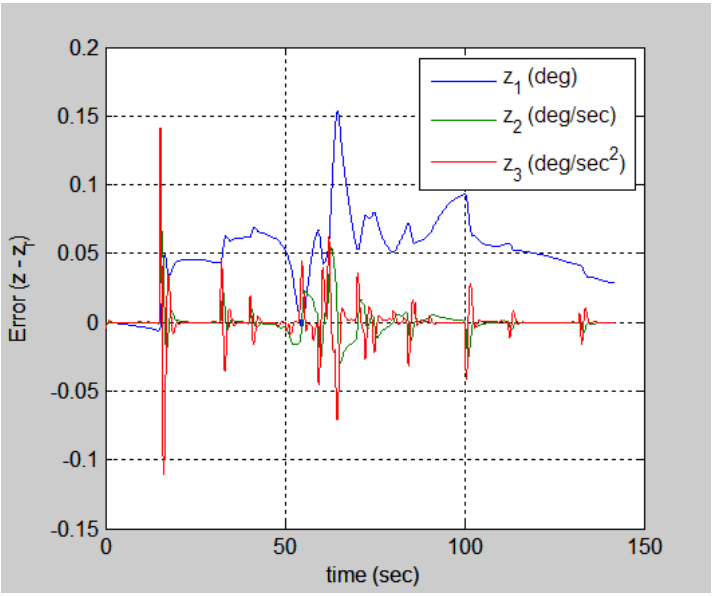

Figure 19. Error Signal Comparison (Baseline Controller)

5.3 MRAC Results

5.3.1 Using Basis Function of Φ(x)

To simulate the adaptive control system, the baseline controller is removed by setting

$$\begin{aligned} K_A &= 1 \\ K_I &= 0 \\ K_R &= 0 \end{aligned} \tag{40}$$

The rate feedback loop in the simulation is also opened as shown in Figure 20. The adaptive design parameters are then chosen as

$$\begin{aligned} \Gamma_r &= 5 \\ \Gamma_1 &= I_{19\times 19} \\ R_1 &= I_{3\times 3} \\ R_2 &= 1 \end{aligned} \tag{41}$$

The basis function, Φ(*x*), is used first and the results at BECO are shown in Table 2.

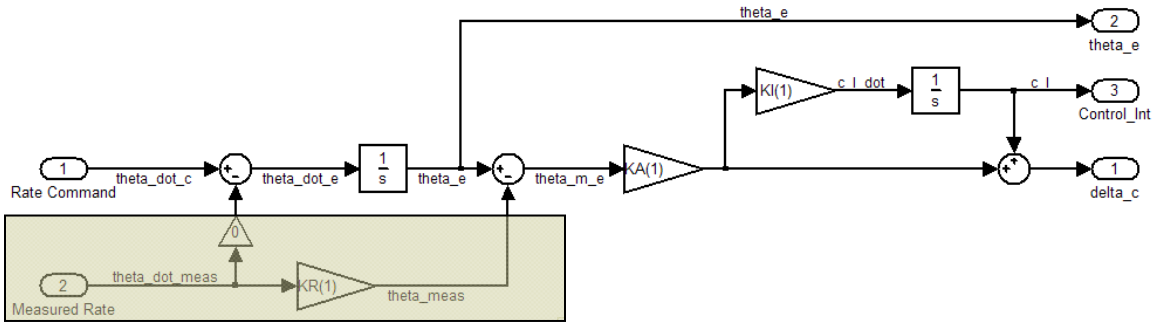

Figure 20. Removal of Baseline Controller in Simulation

Table 2. Simulation Values at BECO (Adaptive Control and Φ(*x*))

Parameter	ELV Simulation	AC-6 Trajectory	Difference
Altitude (ft)	191,870.17	193,784.50	1,914.33
Speed (ft/sec)	8257.31	8245.66	-11.65
Energy (%) [desire ± 0.2%]			0.100

The dynamic pressure comparison in Figure 21 is similar to that found with the baseline controller. The same can be seen in Figure 22 with the engine deflection comparison.

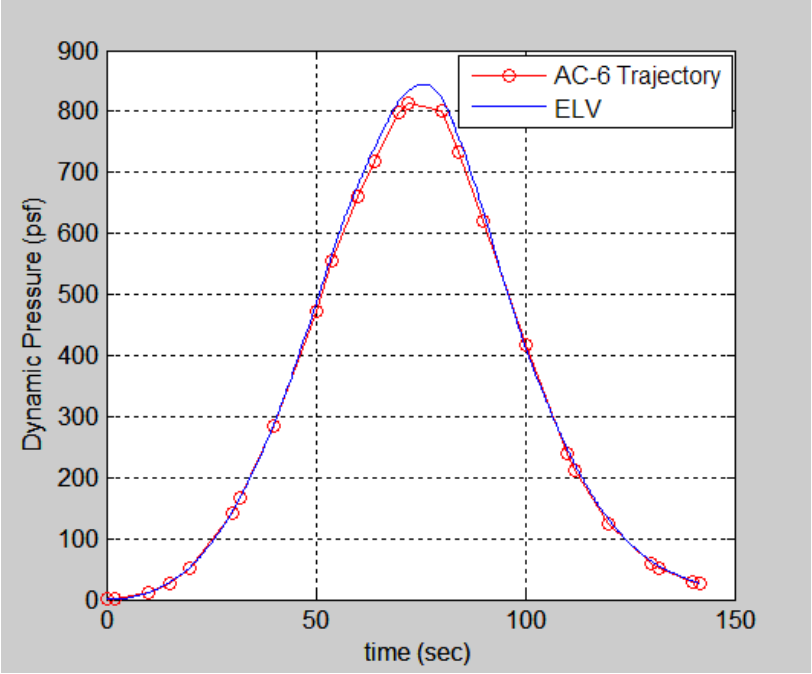

Figure 21. Dynamic Pressure Comparison (Adaptive Controller and Φ(*x*))

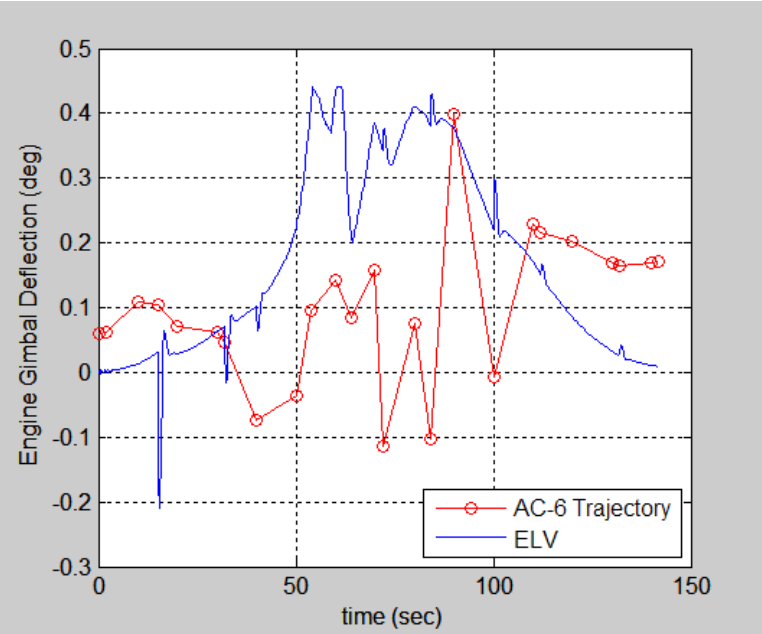

Figure 22. Engine Deflection Comparison (Adaptive Controller and Φ(*x*))

A closer look at the angle-of-attack in Figure 23 shows that the adaptive controller maintains α close to zero in the region of maximum dynamic pressure (t=72 seconds). This result is desired, as aerodynamic loading will be kept to a minimum.

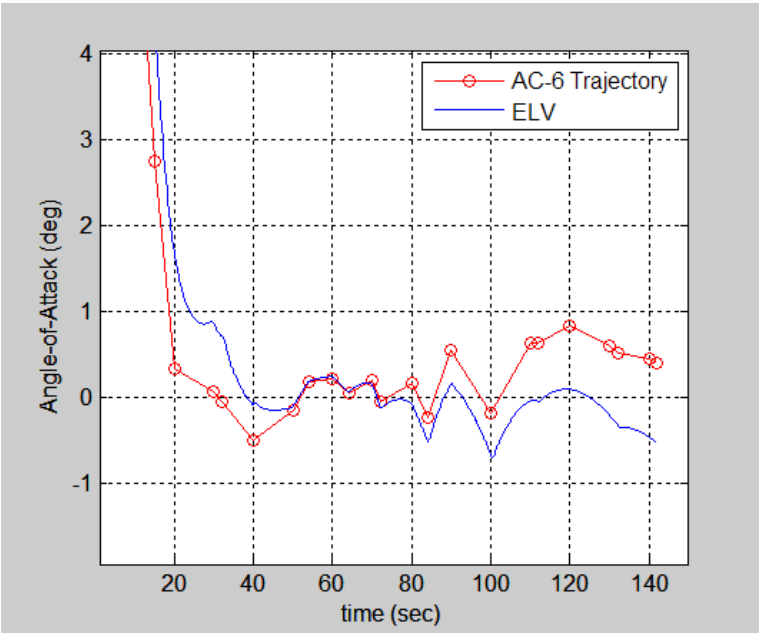

Figure 23. Angle-of-Attack Comparison (Adaptive Controller and Φ(*x*))

Figure 24 and Figure 25 show the altitude and speed respectively along the boost trajectory.

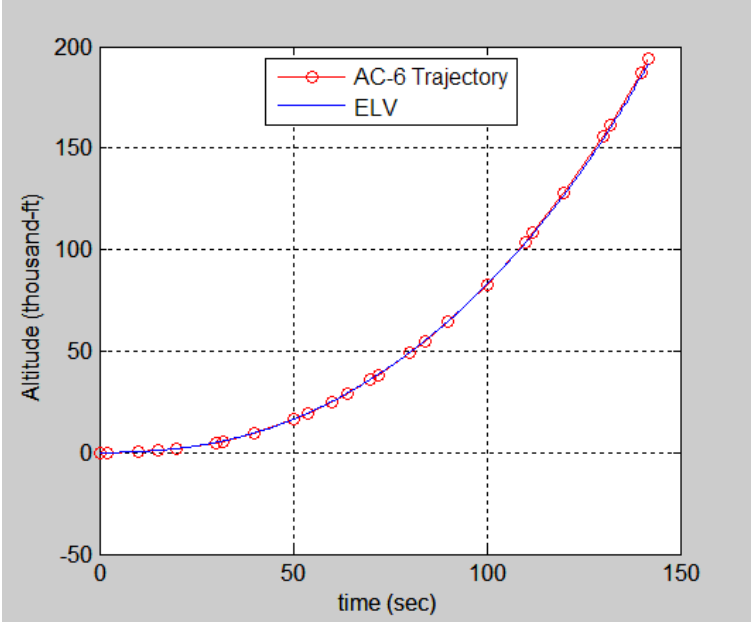

Figure 24. Altitude Comparison (Adaptive Controller and Φ(*x*))

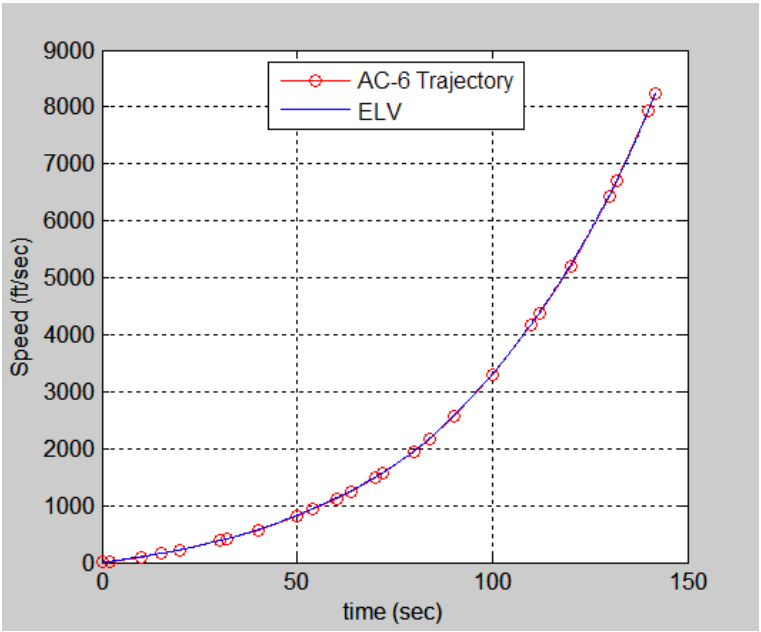

Figure 25. Speed Comparison (Adaptive Controller and Φ(*x*))

Again, the next three figures compare the pitch angular attitude, rate, and acceleration. Notice that in Figure 27 the rate response around the maximum dynamic pressure (t=72 sec) now tracks the commanded rate much better than the baseline controller. Also, Figure 29 shows that the error between the ELV system and the reference model goes to zero after several seconds.

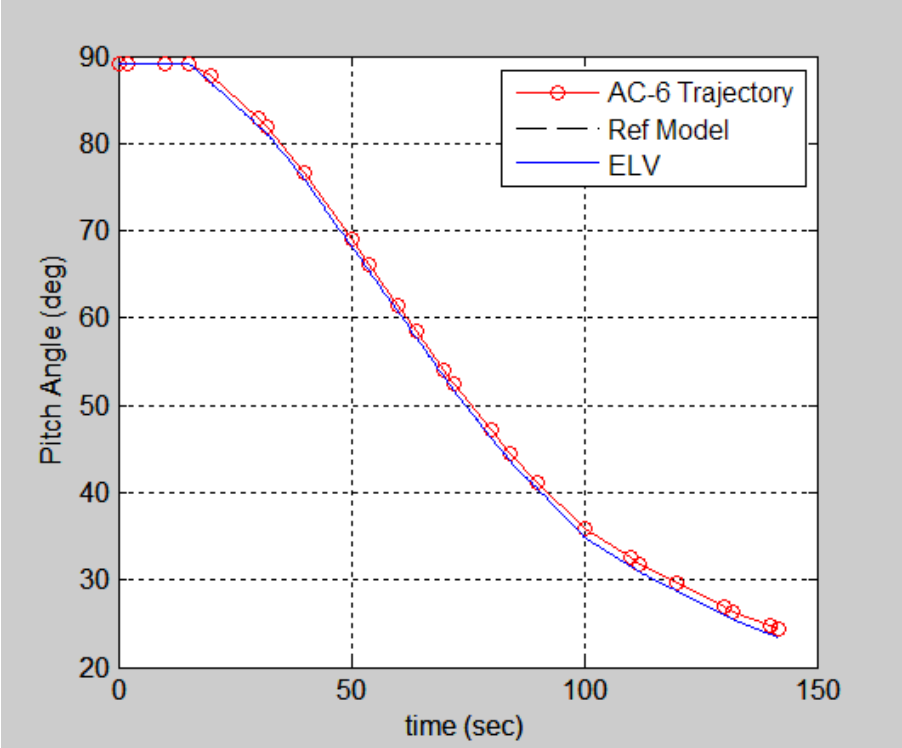

Figure 26. Pitch Attitude Comparison (Adaptive Controller and Φ(*x*))

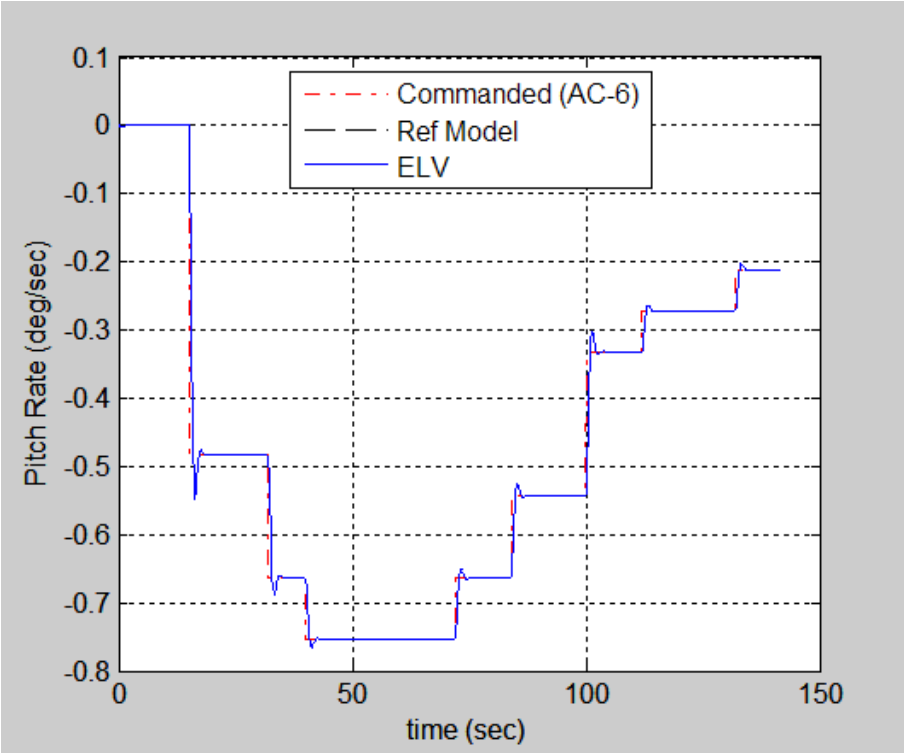

Figure 27. Pitch Rate Comparison (Adaptive Controller and Φ(*x*))

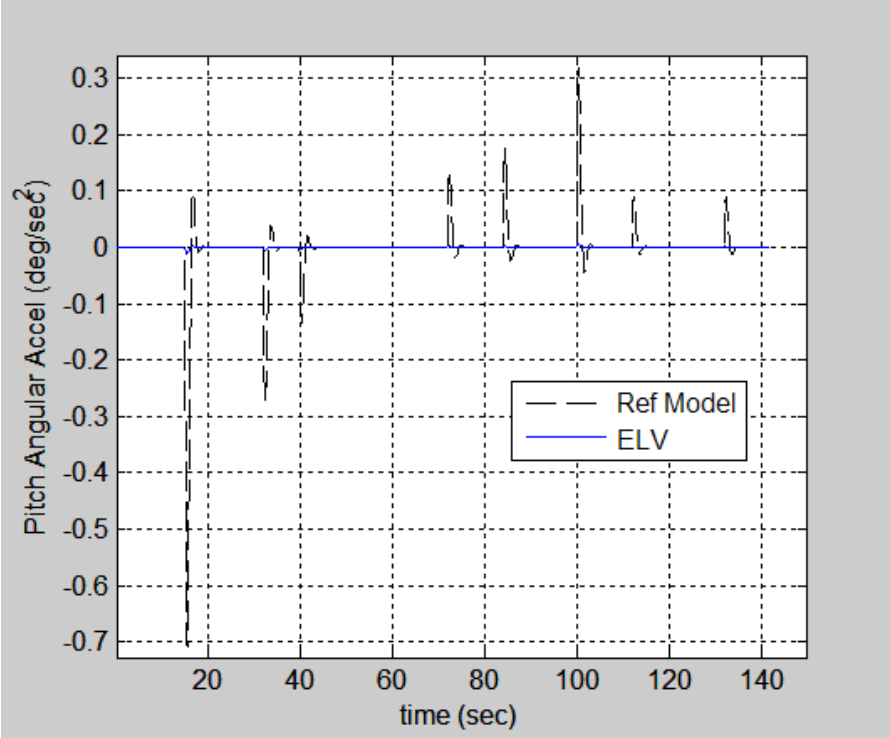

Figure 28. Pitch Angular Acceleration Comparison (Adaptive Controller and Φ(*x*))

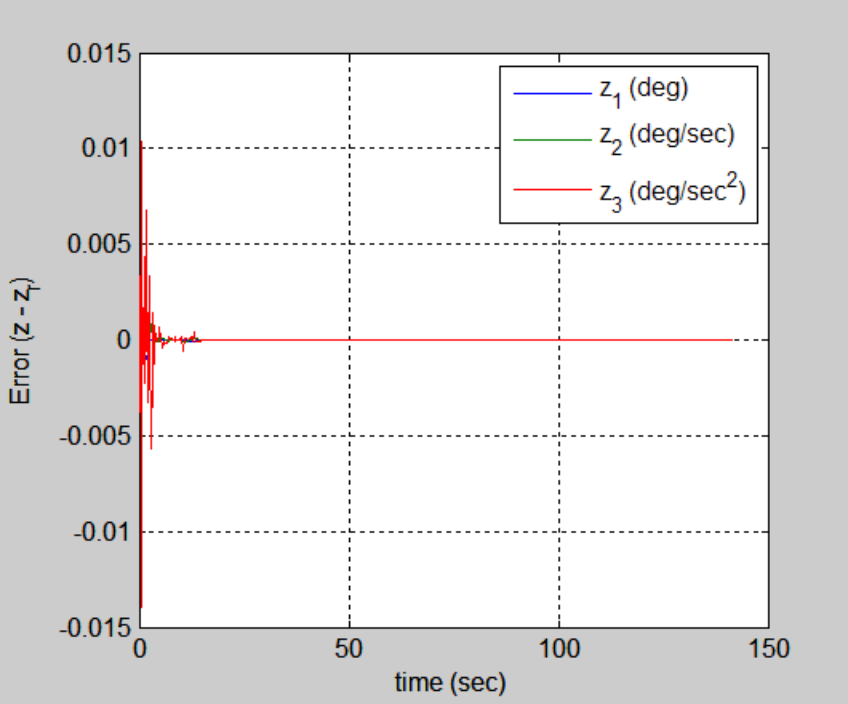

Figure 29. Error Signal Comparison (Adaptive Controller and Φ(*x*))

The 19 parameter estimates of Θ_1 are shown in Figure 30.

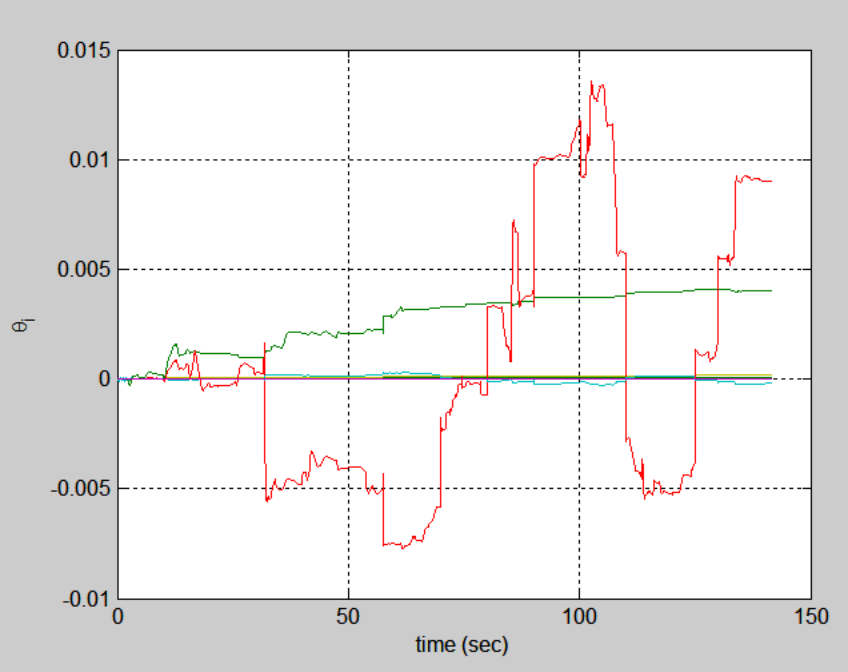

Figure 30. Control Parameters (Adaptive Controller and Φ(*x*))

5.3.2 Using Basis Function of Φ(t,z)

Keeping the same parameters as defined in (40) and (41), but changing the basis function to that of Φ(*t,z*) in (38), the results at BECO are shown in Table 3.

Table 3. Simulation Values at BECO (Adaptive Control and Φ(*t,z*))

Parameter	ELV Simulation	AC-6 Trajectory	Difference
Altitude (ft)	191,814.74	193,784.50	1,969.76
Speed (ft/sec)	8,258.06	8,245.66	-12.40
Energy (%) [desire ± 0.2%]			0.101

The dynamic pressure in Figure 31 is again similar to that found with the baseline controller and that of the adaptive controller with Φ(*x*). The same can also be said of Figure 32 with the engine deflection comparison. The adaptive controller maintains α close to zero in the region of maximum dynamic pressure as well (see Figure 33).

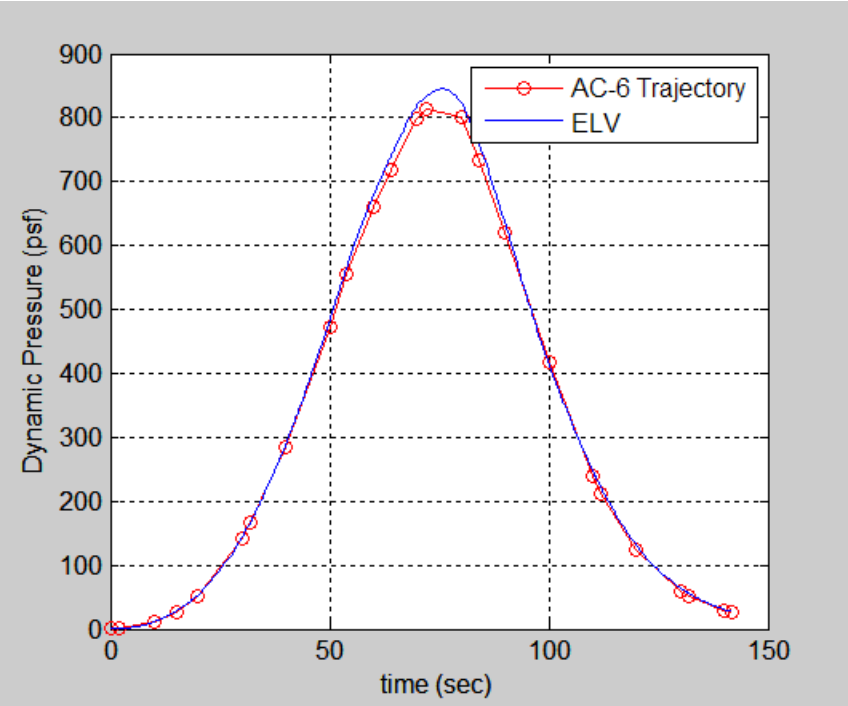

Figure 31. Dynamic Pressure Comparison (Adaptive Controller and Φ(*t,z*))

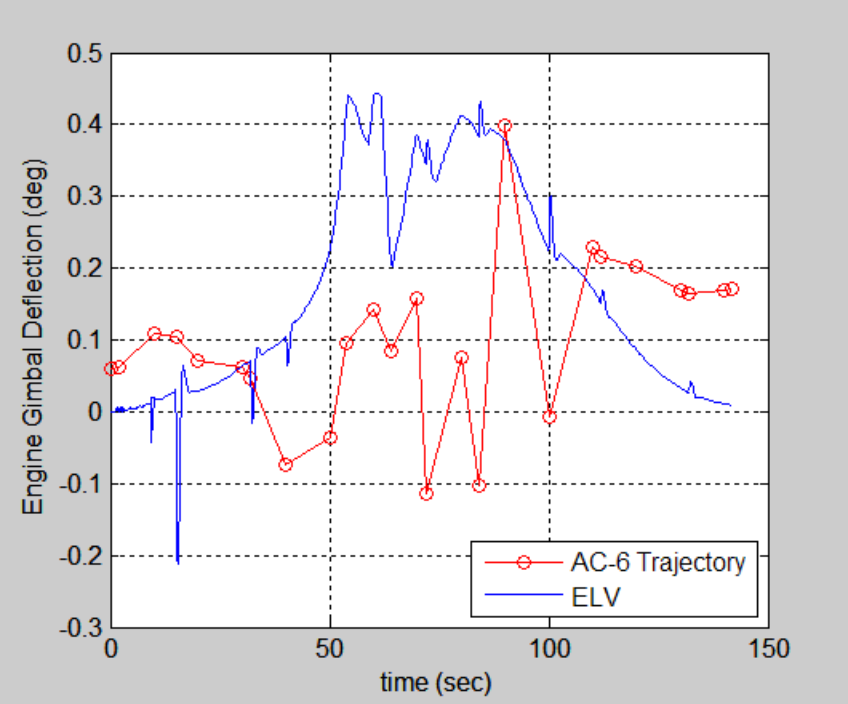

Figure 32. Engine Deflection Comparison (Adaptive Controller and Φ(*t*,*z*))

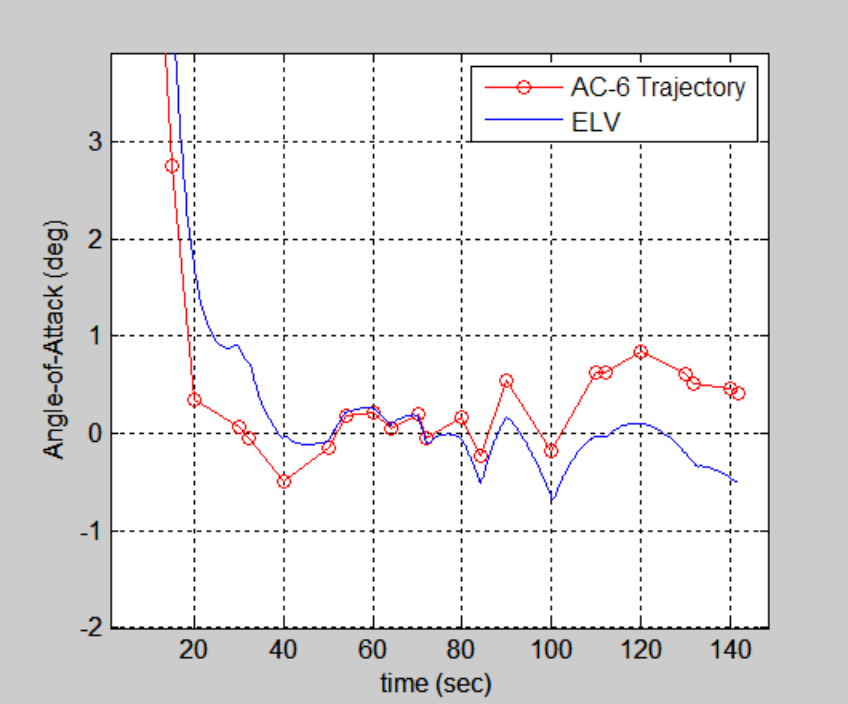

Figure 33. Angle-of-Attack Comparison (Adaptive Controller and Φ(*t*,*z*))

Figure 34 and Figure 35 show the altitude and speed respectively along the boost trajectory. There is no noticeable difference from the case of $\Phi(x)$.

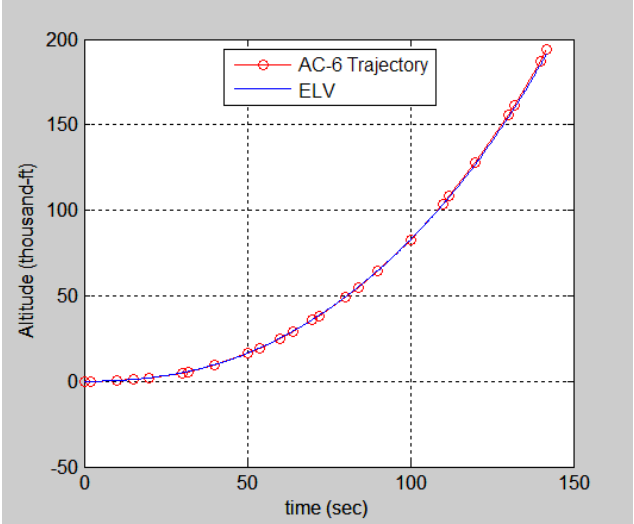

Figure 34. Altitude Comparison (Adaptive Controller and $\Phi(t,z)$)

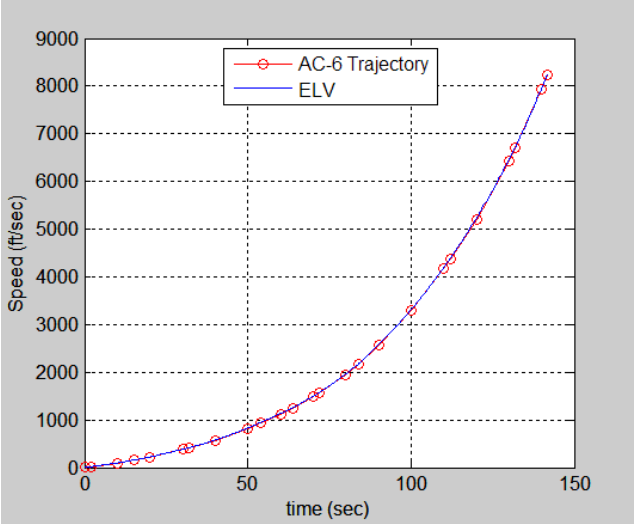

Figure 35. Speed Comparison (Adaptive Controller and $\Phi(t,z)$)

The next two figures compare the pitch angular attitude and rate again. Also, Figure 38 shows that the error between the ELV system and the reference model goes to

zero after several seconds just as in the case of the other basis function simulation. These show that the use of basis function $\Phi(t,z)$ does as well as using $\Phi(x)$.

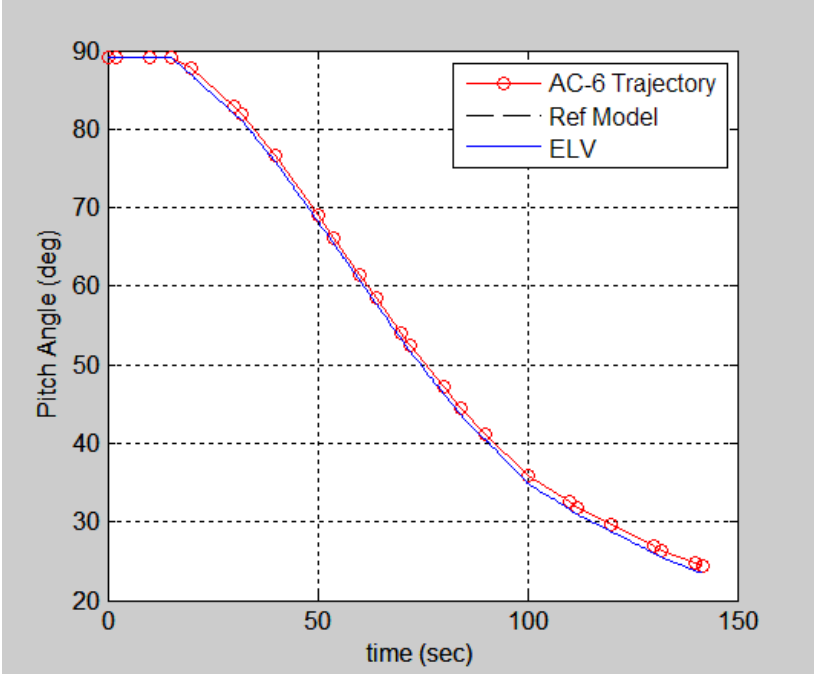

Figure 36. Pitch Attitude Comparison (Adaptive Controller and $\Phi(t,z)$)

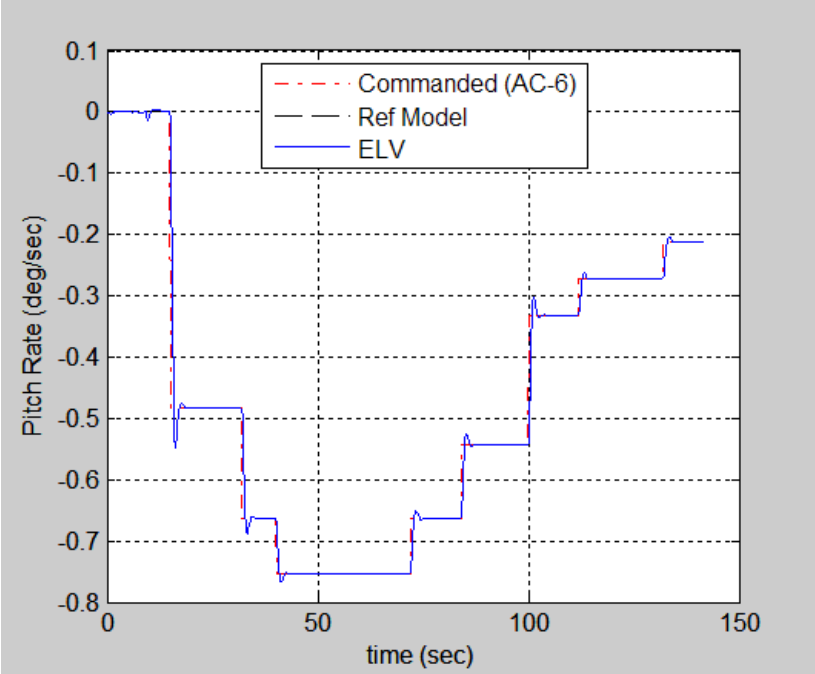

Figure 37. Pitch Rate Comparison (Adaptive Controller and $\Phi(t,z)$)

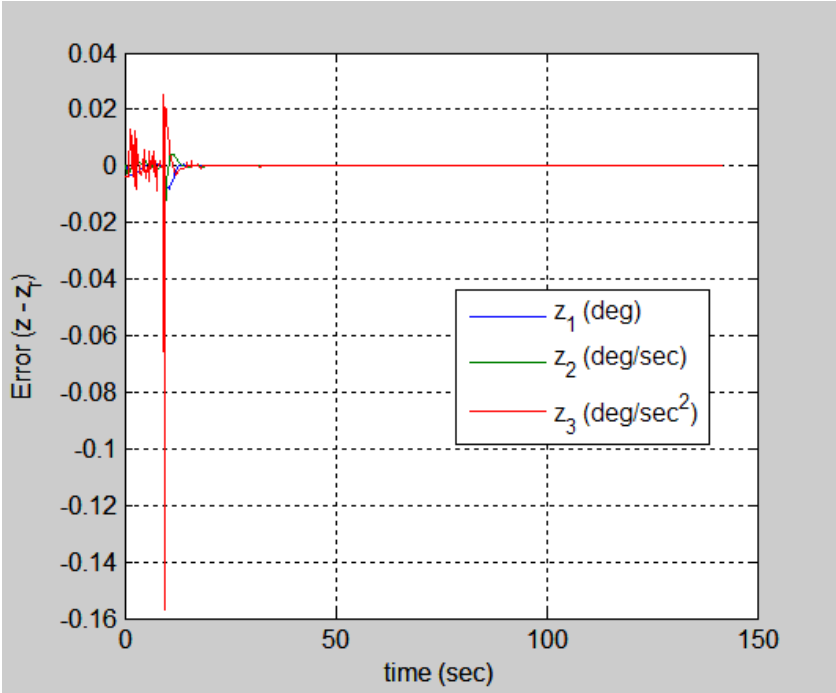

Figure 38. Error Signal (Adaptive Controller and Φ(*t*,*z*))

The 19 parameter estimates of Θ_1 are shown in Figure 39.

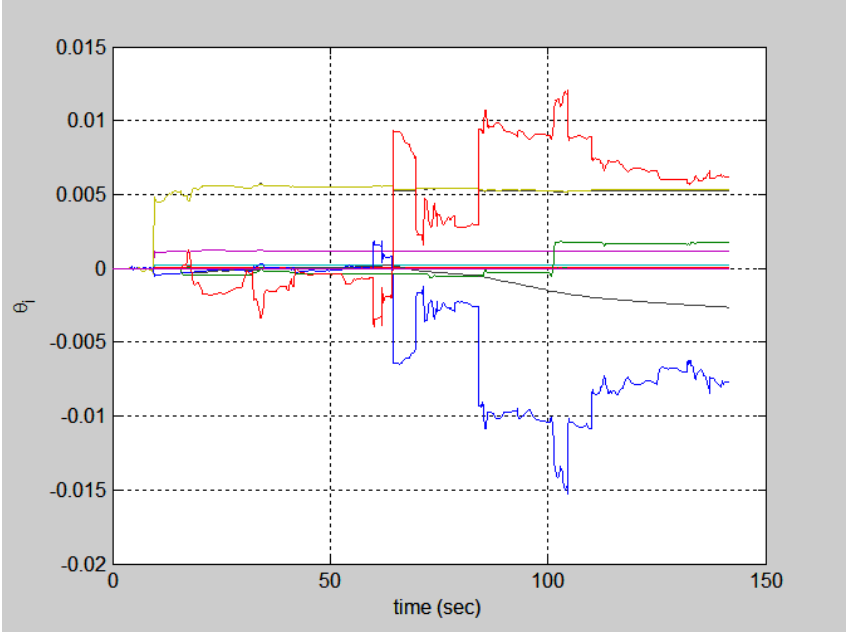

Figure 39. Control Parameters (Adaptive Controller and Φ(*t*,*z*))

5.3.3 Induced Uncertainty

The simulations done in previous sections used nominal ELV parameters of AC-6. To introduce uncertainty in some of the parameters, multipliers on wind and aerodynamic components was implemented. The system was simulated using the adaptive controller with basis function $\Phi(t,z)$ and then with the baseline controller in the presence of the following uncertainties

- Increase CP location and C_N by 50%
- Increase Westerly wind ($-W_E$) by 50%
- Increase CG location by 35%

The BECO comparisons between each controller are shown in Table 4.

Table 4. Comparison of Simulation Values at BECO (with Uncertainty)

Parameter	Baseline Control	AC-6 Trajectory	Difference	Adaptive Control (Φ(t,z))	AC-6 Trajectory	Difference
Altitude (ft)	170217.72	193,784.50	23,566.80	171388.50	193,784.50	22,396
Speed (ft/sec)	8258.88	8245.66	-13.22	8249.60	8245.66	-3.934
Energy (%) [desire ± 0.2%]			-0.005			-0.012

Figure 40 and Figure 41 show the pitch angle achieved with each type of controller. There are slight differences in the attitude values, but the performance is more noticeable in the pitch rate plots of Figure 42 and Figure 43. The adaptive controller tracks pitch rate much better than the baseline controller.

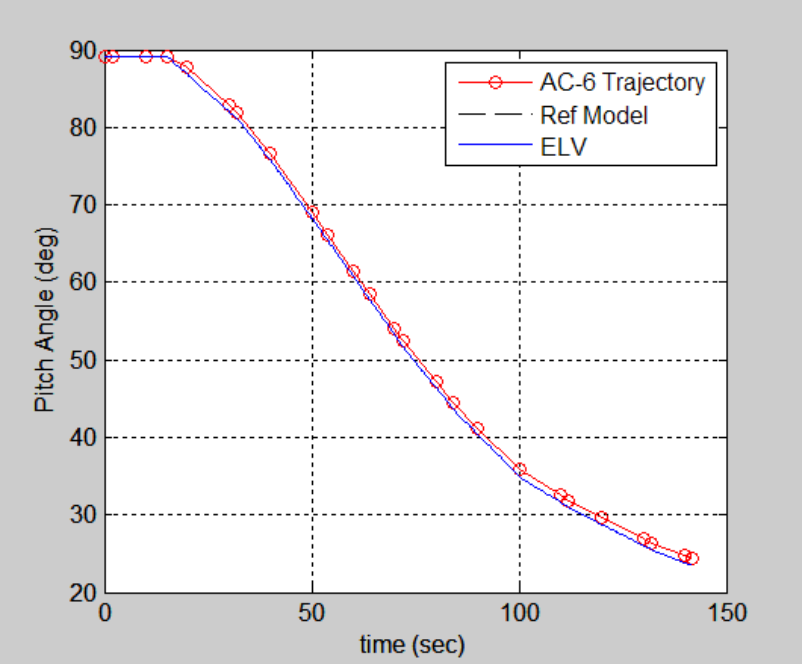

Figure 40. Pitch Attitude Comparison (with Adaptive Controller and Uncertainty)

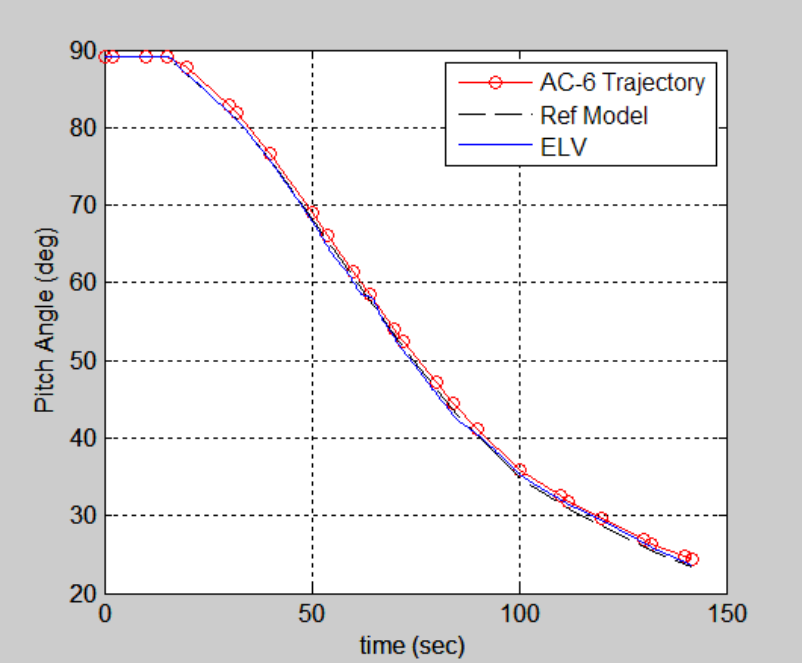

Figure 41. Pitch Attitude Comparison (with Baseline Controller and Uncertainty)

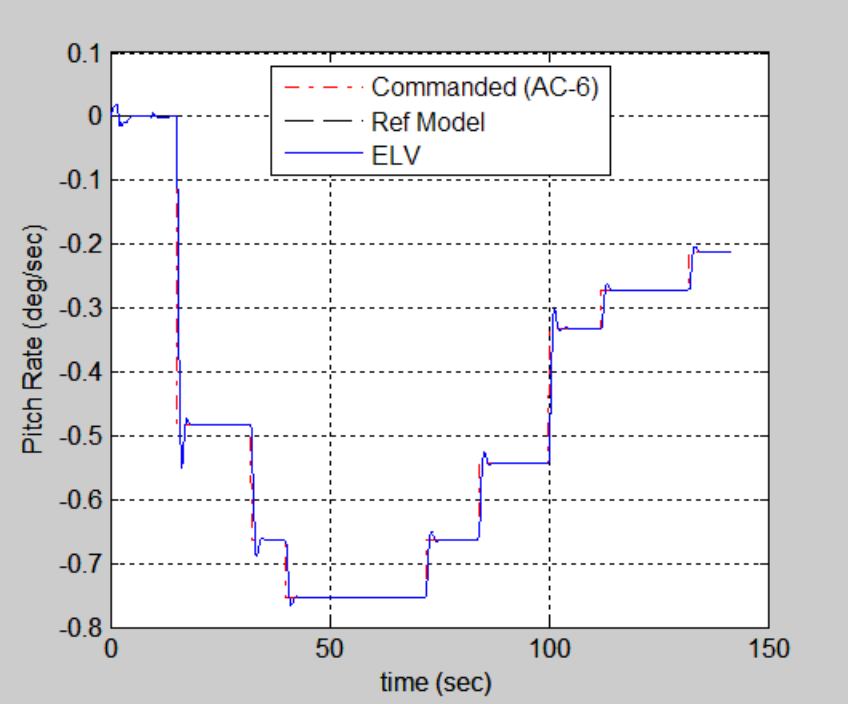

Figure 42. Pitch Rate Comparison (with Adaptive Controller and Uncertainty)

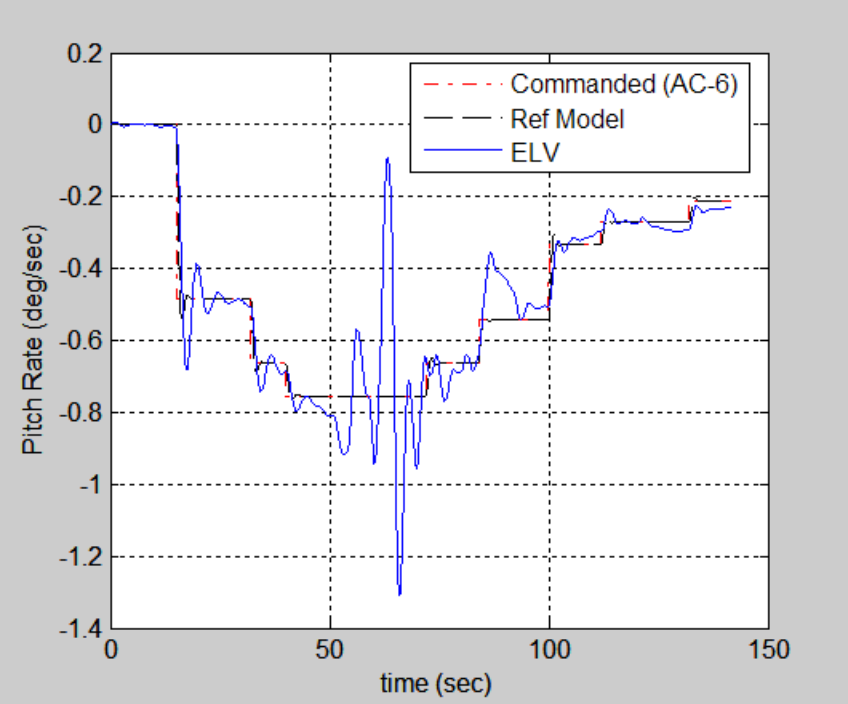

Figure 43. Pitch Rate Comparison (with Baseline Controller and Uncertainty)

The better tracking performance comes with an increase in engine deflection. The next two figures show both the adaptive and baseline controllers have increased engine deflections across the trajectory compared to that of the AC-6 flight.

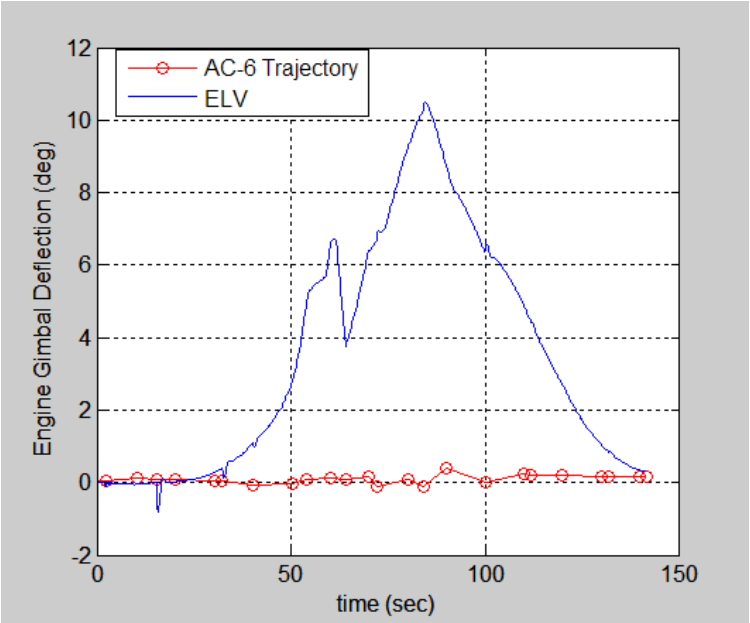

Figure 44. Engine Deflection Comparison (with Adaptive Controller and Uncertainty)

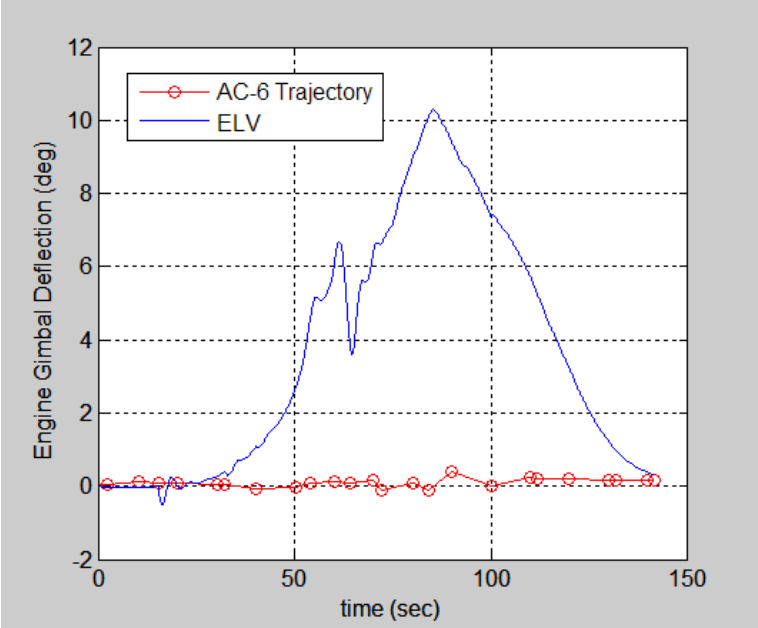

Figure 45. Engine Deflection Comparison (with Baseline Controller and Uncertainty)

The angle-of-attack also increases for both types of controllers (see Figure 46 and Figure 47).

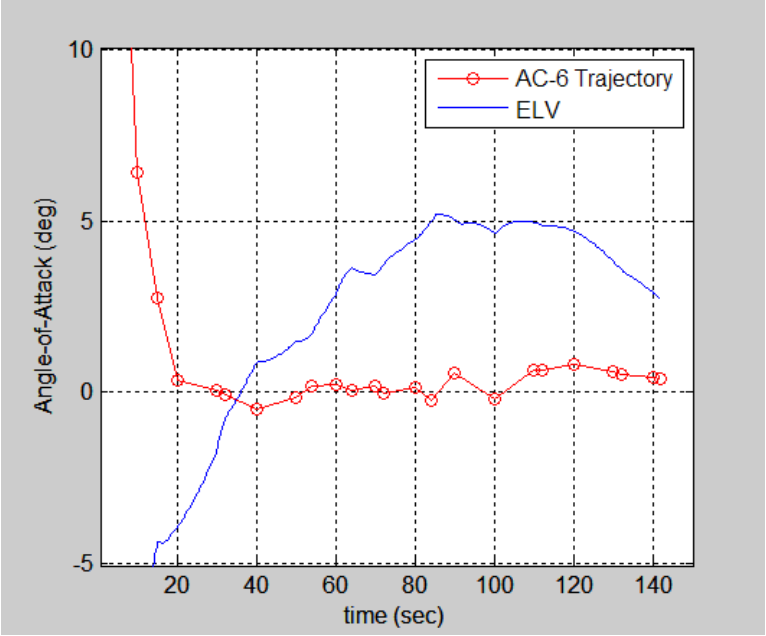

Figure 46. Angle-of-Attack Comparison (with Adaptive Controller and Uncertainty)

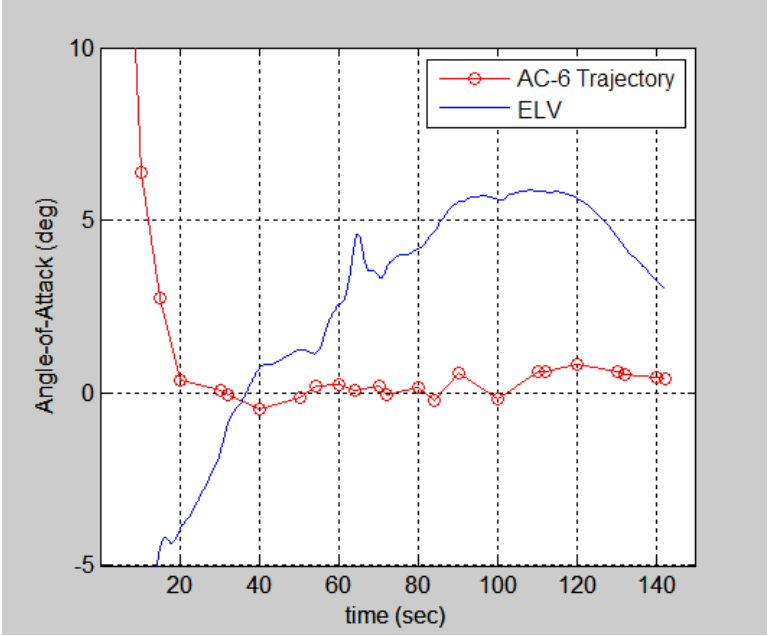

Figure 47. Angle-of-Attack Comparison (with Baseline Controller and Uncertainty)

The increase with angle-of-attack combined with increased dynamic pressure shown in Figure 48 and Figure 49, could lead to unreasonable aerodynamic loading on the vehicle, especially during the maximum dynamic pressure region, for both controller types.

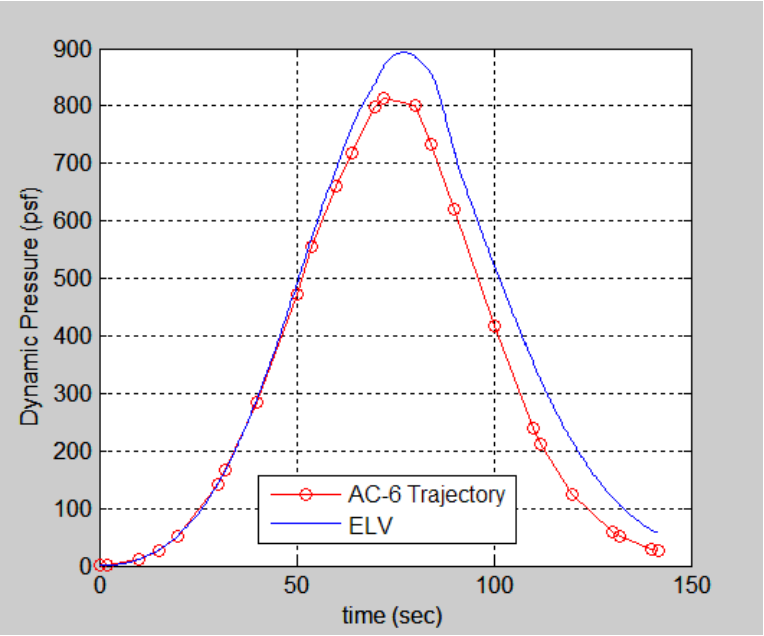

Figure 48. Dynamic Pressure Comparison (with Adaptive Controller and Uncertainty)

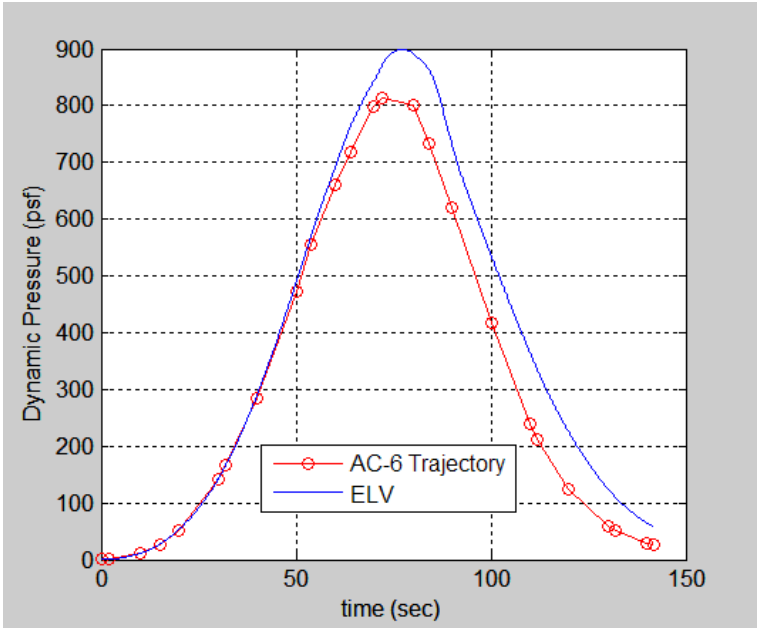

Figure 49. Dynamic Pressure Comparison (with Baseline Controller and Uncertainty)

The pitch angular acceleration is also greater for the baseline controller as seen in Figure 50 and Figure 51.

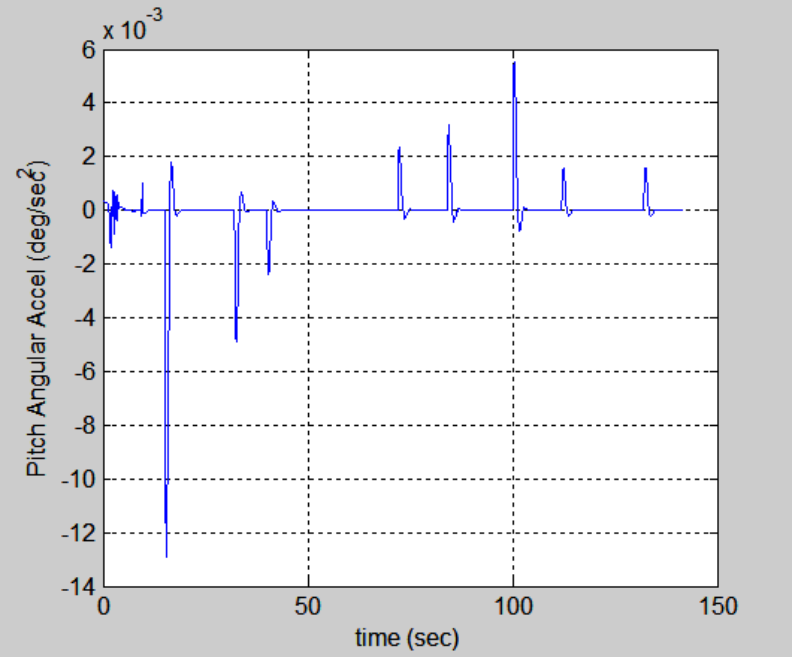

Figure 50. Pitch Angular Acceleration (with Adaptive Controller and Uncertainty)

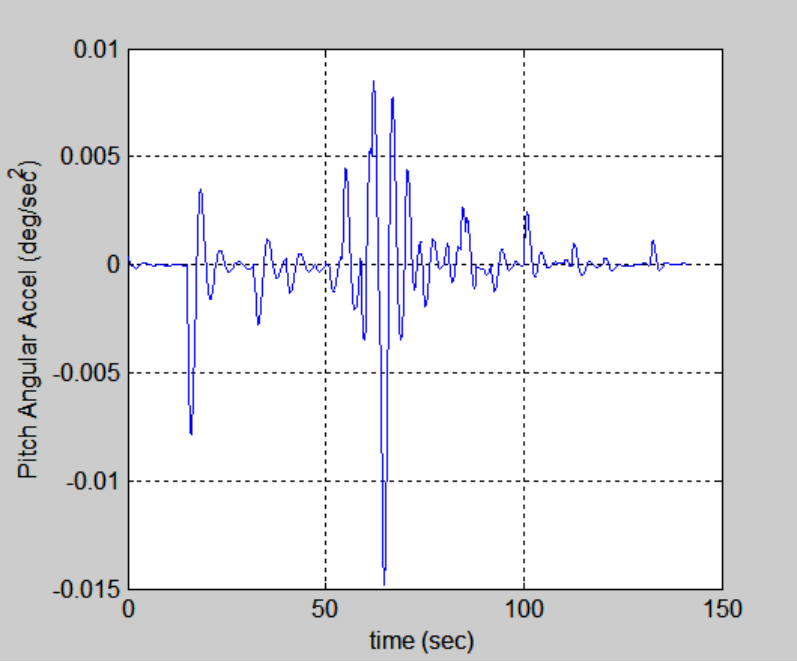

Figure 51. Pitch Angular Acceleration (with Baseline Controller and Uncertainty)

While the speed of the ELV using both the adaptive and baseline controllers doesn't change significantly, the altitude does as seen in Figure 52 and Figure 53.

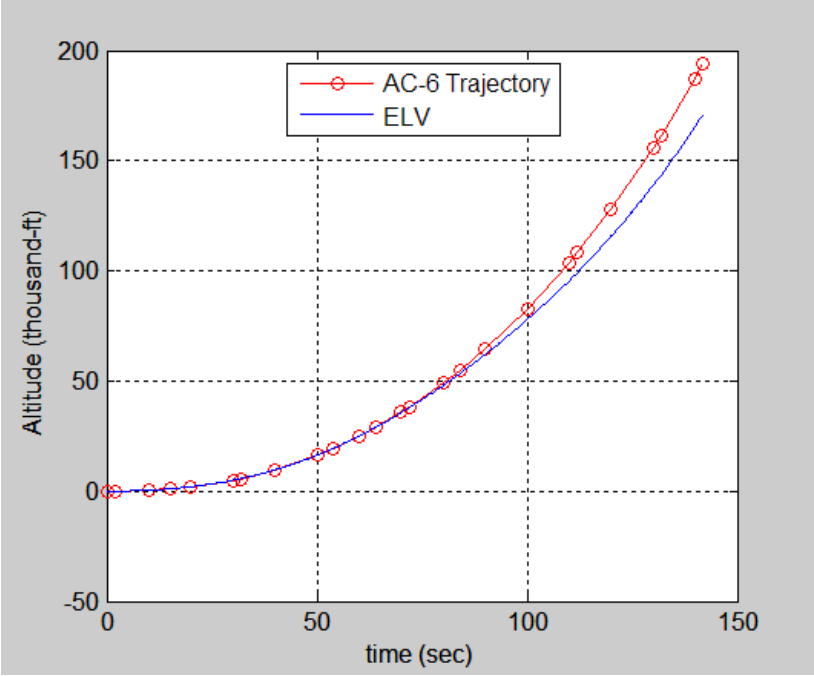

Figure 52. Speed Comparison (with Adaptive Controller and Uncertainty)

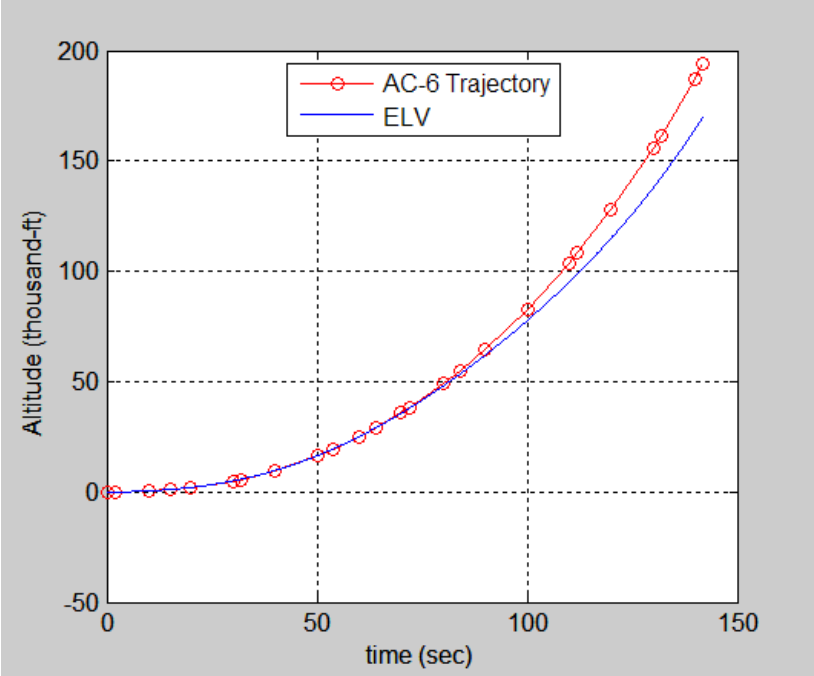

Figure 53. Speed Comparison (with Baseline Controller and Uncertainty)

The error between the adaptively controlled ELV system and the reference model goes to zero after several seconds as expected (see Figure 54). The 19 parameter estimates of Θ_1 are shown in Figure 55.

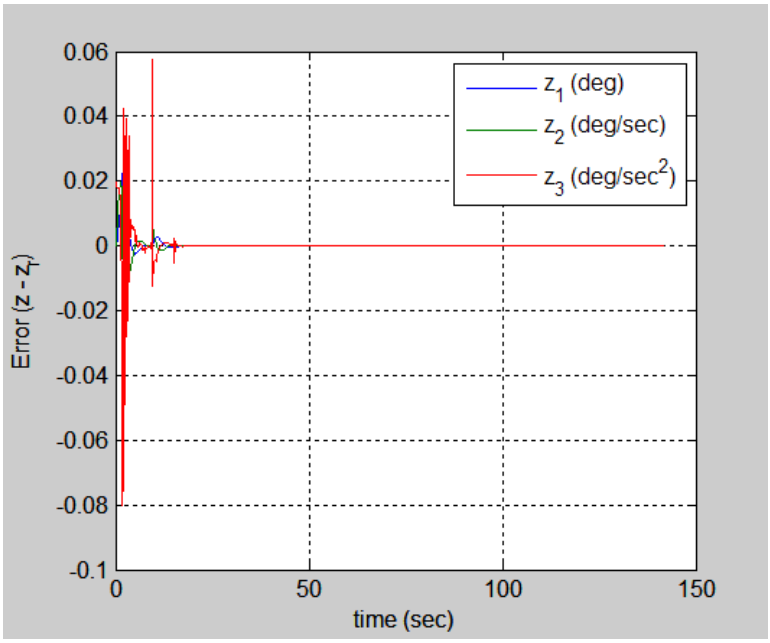

Figure 54. Error Signal (with Adaptive Controller and Uncertainty)

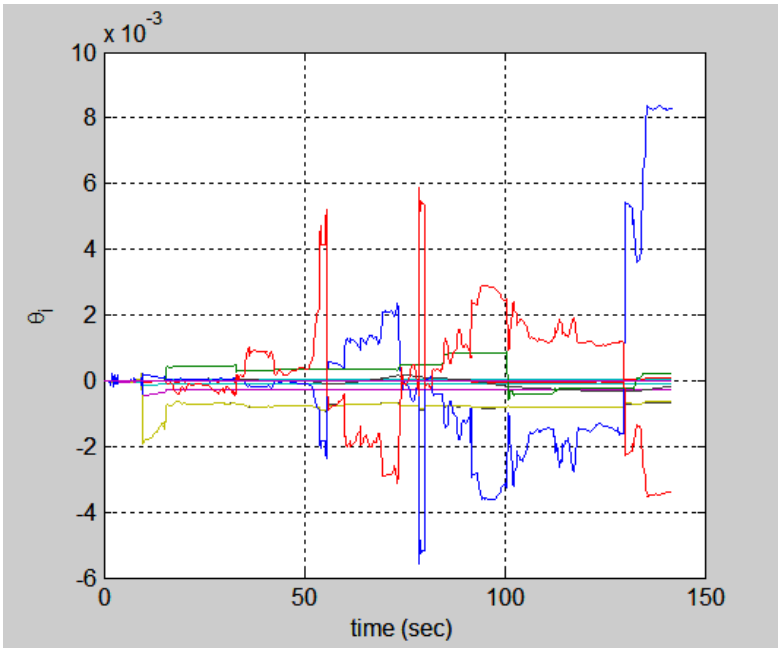

Figure 55. Control Parameters (with Adaptive Controller and Uncertainty)

5.4 Summary

Simulation runs with the baseline controller show that the ELV tracks the rate command sufficiently except in the region of maximum dynamic pressure. Comparisons of the AC-6 trajectory with the chosen reference model also validate its use in the adaptive control system. Two specific sets of basis functions where derived in the previous chapter and each were used in simulating the adaptive control system. Finally, a comparison of the baseline controller with that of the adaptive controller, using the basis function $\Phi(t,z)$, was achieved. The adaptive controller was shown to track the desired pitch rate command much better than the baseline controller with slightly unreasonable uncertainty induced to both simulations. All simulation runs were compared to the trajectory reconstruction for AC-6.

CHAPTER 6: CONCLUSION

The simulation results testing the direct MRAC method have demonstrated that the adaptive control system is robust to uncertainties. Aerodynamics and wind parameters were perturbed and the resulting trajectory was compared to that of AC-6. This thesis has shown that a single adaptive design, that could guarantee stability (or boundedness), could use two different sets of basis functions based on the actual measured states of the ELV. There is no need for gain/filter scheduling of the baseline control. The adaptive controller has shown better tracking of commanded pitch rate than that of the baseline controller in the presence of large uncertainty. This work has shown the merit of direct MRAC applied to ELVs, though more research should be done.

6.1 Future Work

Future research for direct MRAC of ELVs could include solving the attitude control problem with actuator rate and amplitude saturation using [12]. Another direction for study would be to include other ELV dynamics such as bending, slosh, engine inertia, etc. Research done on feedback linearization for flexibly body dynamics was shown in [18].

Other basis functions could also be investigated. The trade between speed and function approximation accuracy should be done to find the most suitable basis functions (e.g. sigmoid functions, radial basis functions, etc.) as well as the number of basis function needed. Also, by including vehicle dynamics such as flexibility and slosh, there will be a need to develop basis functions that can approximate the added uncertain dynamics.

REFERENCES

[1] Astrom, K. J., "Adaptive Control Around 1960", IEEE Control Systems Magazine, June 1996.

[2] Boskovich, B., and R. E. Kaufmann, "Evolution of the Honeywell First-Generation Adaptive Autopilot and Its Applications to F-94, F-101, X-15, and X-20 Vehicles", AIAA Journal of Aircraft, 1966, Vol. 3, No. 4, pp. 296-304.

[3] NASA Flight Research Center Staff, "Experience with the X-15 Adaptive Flight Control System", NASA Technical Note D-6208, March, 1971.

[4] Milton O. and J. R. Welsh, "Flight Test Experience With Adaptive Control Systems", Advanced Control System Concepts, AGARD Conf. Proc. No. 58, Jan. 1970, pp. 141-147.

[5] Greensite, A. L., *Control Theory: Volume II – Analysis and Design of Space Vehicle Flight Control Systems*, Spartan Books, Mcamillan & Co. Ltd., London, UK, 1970.

[6] Blakelock, J.H., *Automatic Control of Aircraft and Missiles, 2nd Edition*, John Wiley & Sons, Inc., NY, 1991.

[7] Lewis Research Center Staff, "Postflight Evaluation of Atlas-Centaur AC-6", NASA TM X-1280, NASA Technical Reports Server, October 1, 1966.

[8] Wilson, L. G. and B. R. Hurlbut, "Postflight Trajectory Reassembly AC-6", NASA-CR-76201, NASA Technical Reports Server, February 18, 1966.

[9] Ohusky, J., and F. Puhn, "External Design Loads for Centaur Vehicles (AC-6 Through AC-15)", NASA-CR-54617, NASA Technical Reports Server, May 1, 1965.

[10] Harris, R., "Atlas-Centaur AC-5 Analog/Digital Load Reduction Autopilot Study", NASA-CR-54487, NASA Technical Reports Server, February, 13, 1964.

[11] Chacon, T., "Distributions and Total Vehicle Aerodynamic Coefficients for the Atlas SLV- 3C Centaur-Surveyor Vehicle", NASA-CR-113387, NASA Technical Reports Server, May 15, 1967.

[12] Leonessa, A., W. M. Haddad, T. Hayakawa, and Y. Morel, "Adaptive Control for Nonlinear Uncertain Systems with Actuator Amplitude and Rate Saturation Constraints", Submitted to International Journal of Adaptive Control and Signal Processing.

[13] Slotine, J-J.E., and W. Li, *Applied Nonlinear Control*, Prentice-Hall, New Jersey, 1991.

[14] Khalil, H. K., *Nonlinear Systems, 3rd Edition*, Prentice-Hall, New Jersey, 2002

[15] Sifer, J.F., S.J. Prouty and P.H. Mak, "Advanced Concepts for Launch Vehicle Control", IEEE AES Magazine, February, 1991.

[16] Wise, K., and E. Lavretsky, "Adaptive Control of Flight: Theory, Applications, and Open Problems", Proceedings of American Control Conference, Minneapolis, MN, June, 2006.

[17] Wise, K., and E. Levretsky, "Robust and Adaptive Control Theory Workshop", AIAA Professional Development Short Course Notes, August, 2006.

[18] Parker, J. T., et. al., "Approximate Feedback Linearization of an Air-breathing Hypersonic Vehicle", Proceedings of the AIAA Guidance, Navigation, and Control Conference, Keystone, CO, August, 2006, Paper AIAA 2006-6556.